| AD NUMBER |
|---|
| AD004960 |
| LIMITATION CHANGES |

TO:

Approved for public release; distribution is unlimited.

FROM:

Distribution authorized to DoD only; Administrative/Operational Use; 02 SEP 1952. Other requests shall be referred to Office of Naval Research, Arlington, VA 22203. Pre-dates formal DoD distribution statements. Treat as DoD only.

AUTHORITY

ONR ltr dtd 26 Oct 1977

# UNCLASSIFIED

# AD _____

## DEFENSE DOCUMENTATION CENTER

### FOR

### SCIENTIFIC AND TECHNICAL INFORMATION

CAMERON STATION ALEXANDRIA, VIRGINIA

# UNCLASSIFIED

A Study of the Ferroresonant Series
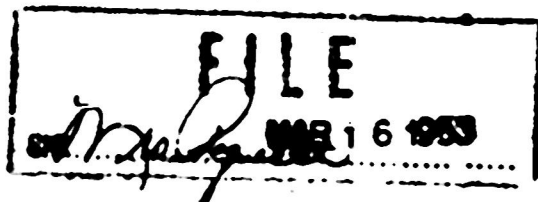Circuit Using Sensitive Core Materials
by Edwin W. Bauer
Research Report R-277-52, PIB-216
Office of Naval Research
Contract N6ori-98, Task Order IV
September 2, 1952

MRI

POLYTECHNIC INSTITUTE OF BROOKLYN
MICROWAVE RESEARCH INSTITUTE

THIS REPORT HAS BEEN DECLASSIFIED
AND CLEARED FOR PUBLIC RELEASE.

ACKNOWLEDGMENT

## ABSTRACT

The applicability of existing methods of solution of the series
ferroresonant circuit when employing sensitive core materials is discussed.
A proposed modification of the Odessey and Weber graphical method of solu-
tion including experimental verification is presented. An analytical analy-
sis of the series circuit based upon the use of a rectangular B-H loop, and
simple criteria for determining the initial current jump point are given.
Also, various modes of circuit operation other than the jump phenomena, which
were experimentally encountered, are discussed. The final sections are
devoted to the use of the series circuit as an amplifier, and the use of
ferroresonance as a means of improving the performance of existing magnetic
amplifier circuits. The experimental results show improvement in both
power gain per cycle and power output of the external feedback and self-
saturating magnetic amplifier circuits.

## Table of Contents                                    Page

R-277-52, PIB-216

Table of Contents

## 1. Methods of Solution for the Series Circuit.

The basic series ferroresonant circuit shown in fig. MRI-12484-a consists of resistance, capacitance and a non-linear inductance. Its fundamental circuit equation for an a-c applied voltage may be written as:

$$e = E_m \sin \omega t = iR + \frac{1}{c} \int i \, dt + N \frac{d\psi}{dt} \; . \tag{1}$$

A first approach to the solution of equation (1) is to represent the B-H curve of the reactor (fig. MRI-12484-b) as a power series such as:

$$H = K_1 B + K_3 B^3 + K_5 B^5,$$

or

$$i = a_1 \psi + a_3 \psi^3 + a_5 \psi^5, \tag{2}$$

and to solve the resulting differential equation. This series must contain only odd power terms in order that it also remain valid for negative values of flux and current. For the low permeability materials, the magnetization characteristics exhibit rounded knees and are usually represented mathematically by a linear term and one power term. Equation (3) represents a compromise between accuracy of solution and the need for simplicity:

$$i = a_1 \psi + a_3 \psi^3. \tag{3}$$

The newly developed sensitive core materials exhibit extremely high permeabilities and sharp knees in their magnetization characteristics. These characteristics approach the form for the ideal B-H curves of fig. MRI-12484-c,d. Fig. MRI-12484-e shows the family of a-c magnetization loops for the sensitive core material Deltamax. The mean magnetization curve passes through the peak flux excursion points of these loops, and for mathematical analysis the curve of fig. MRI-12484-c suffices. Another family of B-H curves is shown in fig. MRI-12484-f for Hypernic V material. Its mean magnetization curve is practically coincident with the outer edge of the large B-H loop. Note that for this material, practically no flux buildup occurs until the coercive force has been established. Therefore, in mathematical treatments of circuits using this material, one should consider use of the ideal B-H characteristic of fig. MRI-12484-c.

When considering use of the sensitive core materials, it is obvious that many higher order terms must be included in the power series (equation 2) in order that an accurate solution be approached. Therefore, a rigorous mathematical solution of this type becomes impossible for the ideal case. Also, with reference to fig. MRI-12484-d,f, it should be

noted that equations (2,3) do not take into account any initial reverse curvature which may occur in the B-H characteristic. Although this initial curvature is negligible for the low permeability materials, it may be of importance with some of the more sensitive core materials as further illustrated by the reactor volt-ampere characteristics of Fig. MRI-12455.

Another approach to the series circuit solution, is to assume that the circuit response is predominantly sinusoidal, thereby allowing a-c impedance concepts to be used. It is necessary that the magnetization curve be fairly linear over the region of operation which normally extends into the saturated portion of the B-H curve. The method is, therefore, applicable to relatively low permeability materials. Even under the condition of large saturation for these materials the magnitude of the third harmonic usually lies between 30-50% of the fundamental, whereas the higher order harmonics are definitely negligible.

## a) Analytical Solution (Thomson Method).

As an analytical example of the above method of solution Thomson's[1] approach is typical. The basic circuit of equation (1) in terms of effective values of current is expressed as

$$E = I (R^2 + X^2)^{1/2}$$

where

$$R = R_o + R_L = \text{external resistance + apparent reactor resistance}$$

$$X = X_L - X_c = \text{total effective circuit reactance}$$

The effective reactance $X_L$ of the saturable reactor is determined from the relationship:

$$R_L^2 = (X_L)^2 = E^2 - (\frac{P}{I})^2 ,$$

and its effective resistance is obtained from

$$R_L = \frac{P}{I^2} ,$$

where P is the measured power consumed by the reactor.

Thomson assumed that the curves of $R_L$ and $X_L$ vs. I (see Fig. MRI-12486-a) could be represented by rectangular hyperbolas given by:

---

[1]  Resonant Non-Linear Control Circuits, W. T. Thomson, AIEE Trans., 57, pp. 469-76, (1938).

$$R_L = \frac{A}{\alpha + I} + K_1,$$

$$X_L = \frac{B}{\beta + I} + K_2,$$

where $A$, $B$, $K_1$, $K_2$, $\alpha$, $\beta$ are reactor constants determined by choosing three points on the curves of Fig. MRI-12486-a. A plot of equation (4) for increasing the values of E and I with $R_o$ as a parameter is constructed in Fig. MRI-12486-b.

Characteristics to be noted which are peculiar only to the series ferroresonant circuit are:

1) Upon reaching a critical voltage, the current takes a sudden jump in value. Experimentally, it has been impossible to attain values for the volt-ampere curve over the region where the slope $\frac{dE}{dI}$ is negative, since this is an unstable region.

2) For resistance values larger than a critical resistance $R_c$ only a single-values response curve can be attained. However, for circuit resistance less than the critical value, a hysteresis type response occurs as illustrated in Fig. MRI-12486-b for $R_L$ $R_o$.

Since the slope $\frac{dE}{dI} = 0$ at two points, and these two points merge into one when the critical resistance is in the circuit, it is possible to solve for the value of critical resistance, critical stable voltage and critical stable current. In order to facilitate the solution, Thomson assumed that the low to high current jump point is independent of resistance. Rouelle[2] states that this condition holds true only for the ideal reactor characteristic. The volt-ampere response curve of Fig. MRI-12487 give experimental verification of this fact. When considering use of the more sensitive core materials, this asumption appears as the only valid portion of the Thomson method.

The rectangular hyperbola representation of Fig. MRI-12486-a is no longer possible with the sensitive materials since one would expect a new $X_L$ vs I characteristic of the form shown in Fig. MRI-12486-c.

To take full advantage of the high permeabilities of the new core alloys (Deltamax, Hypernik V, Orthonik) flux leakage, eddy current, and air gap losses are kept at a minimum by using continuous tape wound cores or extremely thin washer type laminations. Thus, in general, the

---

[2] An Experimental Study of Ferro-Resonance (Contribution a l'etude experimentalle de la ferroresonance), E. Rouelle, Revue Generale de l'Electricite, 36, Nov. 1934, pp. 715-38; Dec. 1934, pp. 763-80; Dec. 1934, pp. 795-819; Dec. 1934, pp. 841-58.

effective resistance can be neglected in circuit calculations and $R_o$ used in place of R.

The greatest objection to the Thomson method is the assumption of sinusoidal quantities, since the harmonic content associated with the ferro-resonant region of high currents is tremendous. The harmonic distribution for a Deltmax core is given in fig. MRI-12489 and is representative of the sensitive core materials. To include consideration of the harmonics in Thomson's method would entail a lengthy and difficult, if not impossible, analysis.

A graphical method of solution for the series circuit investigated by Rouelle, Margand[3], and Odessey and Weber[4] is also based on the assumption of a sinusoidal variation of current. Again the method yields satisfactory results for the low permeability cores, but is unsatisfactory for use with circuits using the sensitive reactors mainly because of neglect of the high order current harmonics.

## b)  Graphical Solution (Odessey and Weber Method)

The graphical method consists of constructing two independent curves for the reactor voltage as a function of reactor current. One relation is obtained directly from the reactor volt-ampere characteristic

$$E_L = f(I),$$

and the other expression for reactor voltage, $E_L$, is obtained from the fundamental a-c circuit equation for the linear series circuit:

$$E = IZ$$
$$= I \sqrt{R^2 + (\omega L - \frac{1}{\omega c})^2}$$

$$E^2 = I^2 R^2 + (E_L - \frac{I}{\omega c})^2$$

$$E_L = \pm \sqrt{E^2 - (IR)^2} + \frac{I}{\omega c} \quad . \tag{5}$$

The first term on the right-hand side of equation (5) is an ellipse having

3

  Au sufet de L'existence de deux regimes en Ferroresonance, F. Margand, Revue Generale de l'Electricite, May 1934, pp. 635-7.

4

  Critical Conditions in Ferroresonance, P.H. Odessey, E. Weber, AIEE Trans., 57, pp. 444-452, (1938)

principal axes of E and E. The remaining term yields a straight line plot having a slope of    K .

$$\theta = \tan^{-1} \left( \frac{1}{\omega c} \right).$$

In order to take into account the effect of the circuit harmonics, Odessey and Weber assumed an empirical frequency correction factor. The corrected frequency term is defined by:

$$\omega^1 = 1.24\omega.$$

Using the Deltamax core whose volt-ampere characteristics appear in fig. MRI-12485 a response curve (fig. MRI-12491) was calculated for the series circuit by means of the graphical method (see fig. MRI-12490). The line voltage was arbitrarily fixed and the capacitance varied in order to obtain the expected hysteresis type response. The current jumps occur whenever a point of tangency is reached between the reactor volt-ampere curve and the elliptic curve for $E_L$.

The calculated response of fig. MRI-12491 is seen to be larger in magnitude and to exhibit a much wider "hysteresis loop" than the experimentally measured response. The difference between the response curves can be attributed to the high order of harmonics which are associated with the high current region of ferroresonant circuits using sensitive core materials. The frequency correction factor of 1.24 assumed for the low permeability materials is no longer valid. Also the graphical construction for $\frac{I}{\omega c}$ should not be represented by a single straight line (see fig. MRI-12486-d). For the high permeability materials, a two-line representation (fig. MRI-12486-e) of the actual volt-ampere characteristic is usually sufficient.

As an example using the above modifications, consider the series circuit of fig. MRI-12484-a in which $R = 300\Omega$, $C = 3\mu f$, $f = 60$cps and the saturable reactor is identical with the Deltamax reactor whose volt-ampere characteristics are shown in fig. MRI-12485.

In fig. MRI-12492 the solution of the circuit was carried out by the Odessey and Weber method. The graphical construction for the proposed modified form of this method is illustrated in fig. MRI-12493. The values for $k_3$, $k_5$ in equation (6) were experimentally measured by means of a harmonic analyzer.

The results obtained by the graphical methods of solution are compared with the experimental response of the circuit in fig. MRI-12494. It is seen that the method of Odessey and Weber again yields a response characteristic having a hysteresis loop much wider than the actual response loop (refer to fig. MRI-12491).

The modified method of solution agrees well with the experimentally determined response, and. in general, this method should provide a more satisfactory solution.

Changing to rms. values

$$\frac{V_{c*}}{I_{*}} = Z_{*} = \frac{1}{c}\left[\frac{\frac{I_1^2}{2} + \frac{k_3^2 I_1^2}{9\omega^2} + \frac{k_5^2 I_1^2}{25\omega^2}}{I_1^2 + k_3^2 I_1^2 + k_5^2 I_1^2 + \ldots}\right]^{1/2}$$

where $k_{\measuredangle} = \dfrac{I_{\measuredangle}}{I_1}$

$\measuredangle$ = order of harmonic;

and

$$I_{*} = \frac{I_1}{\sqrt{2}}\left[1 + k_3^2 + k_5^2\right]^{1/2}$$

$$\therefore \quad X_{c*} = \frac{1}{\omega c}\frac{\left[1 + \frac{k_3^2}{9} + \frac{k_5^2}{25} + \ldots\right]^{1/2}}{\left[1 + k_3^2 + k_5^2 + \ldots\right]^{1/2}} \tag{6}$$

Thus for the graphical construction below saturation, equation (5) is used. Above saturation equation (5) takes on the form

$$E_{L*} = \pm \sqrt{E^2 - (I_{*}R)^2} + I_{*}X_{c*}. \tag{7}$$

Note that there is no change in the graphical representation of the elliptic terms of equations (5) and (7) where as the straight line terms differ by a change in slope.

### c) Modification of the Odessey-Weber Method

Suppose that for the series ferroresonant circuit the following conditions are valid:

a) During operation in low current region, $X_L >> X_c$; $X_L >> R$.

b) During operation in high current region, $X_L << X_c$; $X_L << R$.

Then experimentally it is found that the harmonic distribution in the high current region varies little with appropriate changes in capacitance and also with increasing applied voltage. By introducing additional corrections into the graphical method in order to account for the presence of the high order harmonics, and by determining experimentally the harmonic content of

the circuit after saturation for one value of capacitance, it should be possible to predict the circuit response between the specified limits of capacitance more accurately.

Assuming that a sinusoidal current predominates up to the point of saturation, then direct use of the Odessey-Weber method can be used up to this point. The only change thereafter occurs in the plotting of $\frac{I}{\omega c}$ where now $X_0$ has been modified as follows:

$$v_0 = \frac{1}{c} \int_0^t i\, dt.$$

After saturation assume that

$$i = I_1 \sin \omega t + k_3 I_1 \sin 3\omega t + k_5 I_1 \sin 5\omega t + \ldots$$

$$\therefore \quad v_0 = -\frac{I_1}{c} \left[ \frac{\cos \omega t}{\omega} + \frac{k_3}{3\omega} \cos 3\omega t + \frac{k_5}{5\omega} \cos 5\omega t + \ldots \right]$$

## 2.   Analysis Based Upon an Ideal B-H Curve

The following analysis of the series ferroresonant circuit fig. MRI-12404-a is based upon the use of an ideal three-line B-H curve (fig. MRI-12495-a) closely approximates the rectangular type B-H loops obtained with the more sensitive core materials. Circuit operation is assumed to extend far into the region of saturation. Since there are two distinct linear regions associated with the ideal B-H characteristic, which in terms of the saturable reactor correspond either to infinite or zero reactance, the method of solution followed is that of describing the circuit operation independently for each of the regions (1) and (2), and then applying common boundary conditions in order to relate the two responses.

Consider first that the circuit operation is in region (1) and that the mode of operation is proceeding from negative to positive saturation. Then the basic circuit equation for this region can be written as

$$e = E_m \sin \omega t = N \frac{d\psi}{dt} + \frac{1}{c} \int i_1 dt + i_1 R - V_0 \qquad (8)$$

where

$i_1$ = instantaneous value of the circuit current in region (1)

$V_0$ = initial magnitude of the capacitor voltage upon entering region (1).

Since $i_1 = 0$ for the assumed B-H curve configuration, equation (1) reduces to

$$\text{Em sin wt} = N \frac{d\psi}{dt} - V_0. \tag{9}$$

The choice of an initial negative charge on the capacitor was reasoned as follows. Because of no current flow in region (1), $V_0$ remains constant during the time of operation in this region. Furthermore, since a symmetrical B-H characteristic was assumed, it follows that the magnitude of $V_0$ upon entering region (2) must equal the magnitude of $V_0$ upon leaving that region, although the capacitor charge will have reversed sign due to current flow in region (2). Therefore, since circuit operation was assumed to begin in region (1) at the point of negative saturation, the capacitor charge must be negative due to the prior negative current flow in region (2).

Suppose that region (1) was assumed to possess a small finite slope, then equation (9) would still be valid provided that the reactor impedance in region (1) was much greater than the capacitive impedance or circuit resistance.

Integrating equation (9) over region (1), we obtain

$$\int_{t_1}^{t_2} \text{Em sin } \omega t = \int_{-\psi s}^{\omega s} Nd \quad - \int_{t_1}^{t_2} V_0 \, dt; \tag{10}$$

where

$t_1$ = time of leaving negative saturation region (2)

$t_2$ = time of leaving region (1) and entering, positive saturation region (2)

$$\therefore \quad \frac{-\text{Em}}{\omega} \cos \omega t_2 + \frac{\text{Em}}{\omega} \cos \omega t_1 = N2\psi_s - V_0 (t_2 - t_1).$$

Let $\omega t_1 = \theta_1$, $\omega t_2 = \theta_2$

Then for region (1)

$$\text{Em} (\cos \theta_1 - \cos \theta_2) = N2\psi_s \omega - V_0 (\theta_2 - \theta_1) \tag{11}$$

The basic equation for region (2) is of the same form as equation (8)

$$\text{Em sin } \omega t = i_2 R + \frac{1}{c} \int i_2 \, dt - V_0$$

where:

$i_2$ = instantaneous value of the current in region number 2.

Applying the common boundary conditions at $t_2$, operation in region number 2 dictates that

$$\text{Lim} \left[ \int_{(t_2 - \varepsilon)}^{(t_2 + \varepsilon)} i_2 \, dt \right] = 0 \text{ as } \varepsilon \to 0.$$

Thus we obtain for region number 2

$$Em \sin \theta_2 = i_2 R - V_0 . \tag{12}$$

Note that $i_2$ need not be zero at time $t_2$.

Similarly at time $(t_1 + \frac{\pi}{\omega})$ the lim $\begin{bmatrix} (t_1 + \frac{\pi}{\omega} + \epsilon) \\ \int i_2 \, dt \\ (t_1 + \frac{\pi}{\omega} - \epsilon) \end{bmatrix}$ = as $\epsilon \to 0$. $\tag{13}$

$$Em \sin (\theta_1 + \pi) = + V_0 + i_2 R.$$

Because of the difficulty in determining the proper values of $i_2$ at time $t_2$ and $(t_1 + \frac{\pi}{\omega})$ in equations (12) and (13) respectively, a formal solution is prohibitive. Therefore, let us further assume that $R = 0$. Then equations (12) and (13) may be rewritten as

$$Em \sin \theta_2 = -V_0 , \tag{14}$$

$$Em \sin (\theta_1 + \pi) = + V_0 . \tag{15}$$

Expanding (15)

$$\sin \theta_1 \cos \pi + \cos \theta_1 \sin \pi = \frac{V_0}{Em} ;$$

$$Em \sin \theta_1 = - V_0 . \tag{16}$$

From equations (14) and (16) we obtain the significant result

$$\sin \theta_1 = \sin \theta_2 \tag{17}$$

Thus the circuit current and applied voltage waveforms will be as shown in Fig. MRI-12495-b. Substituting for $V_0$ in (11), then

$$Em (\cos \theta_1 - \cos \theta_2) = \omega 2N \psi_s + Em \sin \theta_2 (\theta_2 - \theta_1).$$

Since from (17) it follows that

$$\cos \theta_1 = - \cos \theta_2 ;$$

$$-2 Em (\cos \theta_2) = \omega 2N \psi_s + Em (\theta_2 - \theta_1) \sin \theta_2 . \tag{18}$$

Also

$$(\theta_2 - \theta_1) = (\pi - 2\theta_1)$$

$$\theta_2 = (\pi - \theta_1).$$

Note that the restrictions on $\theta_1$ are:

Substituting in (18)                    $-\dfrac{\pi}{2} \geqslant \theta_1 \geqslant 0$

$$2Em \cos \theta_1 = 2\omega N\psi_s + Em \sin \theta_1 (\pi - 2\theta_1),$$

$$Em = \dfrac{\omega 2N\psi_s}{2\cos \theta_1 - (\pi - 2\theta_1)\sin \theta_1} \tag{19}$$

The capacitor voltage $V_o$ can be determined from equation (16). However, it may also be determined from the relation that

$$+\overline{V}_o = -V_o + \dfrac{1}{c}\int_{t_2}^{t_1 + \frac{\pi}{\omega}} i_2 \, dt \qquad ,$$

$$V_o = \dfrac{1}{2c}\int_{t_2}^{t_1 + \frac{\pi}{\omega}} i_2 \, dt. \tag{20}$$

Rewriting (19) in terms of half-cycle average values where

$$Em = \overline{E} \pi,$$

then

$$\overline{E} = \dfrac{4\Upsilon N\psi_s}{2\cos \theta_1 - (\pi - 2\theta_1)\sin \theta_1} \tag{21}$$

Similarly from (20) we obtain the half-cycle average current

$$\overline{I}_2 = \dfrac{\omega 2cV_o}{2\pi} = \dfrac{\omega}{2\pi}\int_{t_2}^{t_1 + \frac{\pi}{\omega}} i_2 \, dt \tag{22}$$

Combining (16) and (22)

$$\overline{I}_2 = \omega c\overline{E} \sin \theta_1. \tag{23}$$

Response Curve Calculations for Deltamax Core: - (see Fig. MRI-12496)

$\psi_s$ = 39600 lines

N = 700 turns

f = 60 cps

c = 3 $\mu f$

$$E = \frac{4fN \psi_s \times 10^{-8}}{\left[2 \cos\theta_1 - (\pi - 2\theta_1) \sin\theta_1\right]} \text{ volts.}$$

$$\left[E = \frac{62.7}{\left[ \qquad \right]}\right]$$

$$\bar{I}_2 = \omega c E \sin\theta_1 \text{ amperes}$$

$$\boxed{I_2 = 1.13 \ E \sin\theta_1 \text{ milliamperes}}$$

| $\theta_1$ | $\cos\theta_1$ | $\sin\theta_1$ | $E$ (volts) | $I_2$ (ma.) |
|---|---|---|---|---|
| $0^\circ$ | 1 | 0 | 31.3 | 0 |
| $5.7^\circ$ | .995 | .099 | 36.7 | 4.1 |
| $11.4^\circ$ | .98 | .197 | 44.1 | 9.8 |
| $22.8^\circ$ | .922 | .388 | 67.0 | 29.4 |
| $34.2^\circ$ | .827 | .561 | 111.0 | 71 |

The significant results of this analysis are:

a) Only a single valued response curve of $E$ vs $I$ is possible since $\frac{dE}{d\theta}$ does not yield multiple jump points. A typical response curve is illustrated in Fig. MRI-12496 versus an experimentally determined curve. (See Fig. MRI-12497 also.)

b) The saturating angles $\theta_1$, $\theta_2$ are independent of the value of capacitance.

c) The value of $E$ for initial operation in region number 2 is independent of capacitance and is equal to the average saturation voltage of the reactor.

d) The value of $I_2$ increases linearly with C. Infinite capacitance would produce an infinite current.

e) This analysis does not necessarily hold when a small finite resistance is present in the circuit.

Since a zero resistance circuit is physically impossible to attain, experiments were made with a Deltamax reactor having an eight ohm winding resistance in an attempt to determine the validity of this analysis. The following significant facts were obtained:

a) For very small values of circuit resistance the initial saturating angle $\theta_2$ was independent of the value of capacitance. Saturating

acteristic for the low current region including the point of the initial current jump.

First consider the case of core materials possessing a mean magnet - ization characteristic similar to that illustrated in Fig. MRI-12499-a. In general, an ideal three line segment curve can be used as a good approximation of the actual characteristic. Note than a flux buildup does not occur unless there is an accompanying change in the magnetizing force.

Curve 1 in Fig. MRI-12498 illustrates the case for $X_c \gg X_L$ and $X_c \gg R$ in region (1); it assumes a capacitive impedance characteristic throughout the entire circuit operation and so no jump points are possible.

When operation keeps within the specified limits it is apparent from the response curves of Fig. MRI-12498 that the initial jump point is definitely a function of the circuit capacitance. As the capacitance is increased, the initial jump point occurs at larger values of applied voltage. For the ideal circuit, the value of capacitance has no effect on the position of the jump point.

As the value of capacitance approaches infinity, a limit voltage $E_s$ is approached beyond which point a jump is no longer realizable, the resultant characteristic now assuming the form of the volt-ampere response for an R-L circuit (see Fig. MRI-12499-b) for which $E_s$ is the voltage necessary for saturation of the reactor.

It is to be noted that the width of the "hysteresis" response loops increases for decreasing values of capacitance. It can also be decreased by increasing the circuit resistance (Fig. MRI-12497). However, the initial jump point is seen to be practically independent of the value of resistance.

For the specified circuit limitations, it is possible to neglect the circuit resistance. Considering operation only in region (1), the series circuit can be represented up to the point of saturation by a linear inductance in series with a capacitor (Fig. MRI-12499-c).

Applying sinusoidal circuit analysis, we can write

$$E = E_L - IX_c. \tag{24}$$

The reactor voltage will be given by the expression

$$E_L = E + E_c = IX_L$$

$$E_L = \frac{E X_L}{(X_L - X_c}$$

Letting $E_s$ = saturation voltage for the coil (fig. MRI-12499-d) then saturation or the initial jump point occurs when

$$E = \frac{E_s(X_L - X_c)}{X_L} = I_s (X_L - X_c) \tag{25}$$

For $X_c = 0$, then $E = E_s$. Thus the applied voltage must be of magnitude equal to the saturation voltage for the coil. This corresponds to the limiting voltage $E_s$ as previously mentioned.

It can be seen from equation (25) that as the capacitive reactance is increased, the magnitude of applied voltage necessary to cause saturation of the reactor decreases. Theoretically when $X_L = X_c$ it would take zero applied voltage to saturate the core.

b) Calculation of the Initial Jump Point.

In computing the low current region response curves, the following procedure is used:

a) A value of I is chosen from the reactor volt-ampere characteristic.

b) $E_L$ is thereby specified.

c) E is computed from equation (24).

d) $E_s$ and $X_L$ or $I_s$ are determined from reactor volt-ampere characteristic.

e) The value of E necessary for the initial jump point is calculated from equation (25).

Computations were made for the series circuit using a Deltamax core. A typical result is shown in fig. MRI-12500 and it is seen that it compares quite favorably with the experimental curve. The small deviations which occur in the vicinity of the initial jump point may be attributed mainly to the neglect of the third harmonic component of the current, which usually rises rapidly in this region, (refer to fig. MRI-12489) and to a lesser degree the omission of circuit resistance in the calculations.

In summarizing, it is seen that one function of the capacitance in the series circuit is to aid the supply voltage in furnishing voltage integral to the reactor. It is possible that the phenomena of ferroresonance, including the "hysteresis" response, may be explained qualitatively as follows. Assuming circuit operation in the low current region, the current

will increase slowly with increasing applied voltage until the capacitor and
applied voltage furnish together enough voltage integral to saturate the core.
At this point an abrupt rise in current causes an increase in the voltage
integral supplied by the capacitor. This increase in the voltage integral
tends to drive the reactor farther into saturation and this in turn causes
the current to increase still further. This effect is cumulative and con-
tinues until the core is fully saturated and the current is limited only by
the circuit resistance and capacitive impedance. Once circuit operation ex-
tends into the high current region, a decrease in the applied voltage does
not necessarily result in an immediate return to operation in the low current
region. The width of the hysteresis loops observed in the experimental curves
of figs. MRI-12497 and MRI-12498 may be explained as the inability of the
capacitor to discharge quickly due to a long time constant $(L/R)$ as compared
with $(1/f)$. Experimentally it is observed that for decreasing values of re-
sistance, the loop width increases. Likewise, decreasing the capacitance in-
creases the amount of voltage integral supplied by the capacitor, thereby
tending to increase the loop width. Thus the circuit operation will remain
in the high current region until the applied voltage together with the cap-
acitor voltage are unable to provide the necessary voltage integral to sat-
urate the core. Operation will then return abruptly to the low current re-
gion.

The core materials which possess rectangular hysteresis character-
istics such as Hypernik V have mean magnetization curves similar to that
shown in fig. MRI-12485. This curve can be idealized somewhat by assuming
a five line segment characteristic as illustrated in fig. MRI-12489-e in
which region (3) may have a zero or finite slope depending upon the initial
permeability characteristics. The initial region (3) of low permeability
is important in that the series circuit operation behaves differently from
that previously described for variations in capacitance when this region is
present. For the case of the Deltamax core, an increase in capacitance
caused a shift in the jump point from a corresponding applied voltage (which
was lower than the normal reactor saturation voltage) toward the saturation
voltage. However, when a Hypernik V core is used, the jump point is shifted
from a corresponding applied voltage, which is greater than the saturation
voltage, back to the saturation voltage point. See fig. MRI-12501.

For the idealized magnetization curve of fig. MRI-12499-e it is
apparent that no flux buildup can occur until the magnetization force attains
the value of the coercive force. The current in region (1) (assuming
nearly infinite slope) will be nearly rectangular in shape and will possess
a discontinuity in region (3). Consequently when the circuit operation
enters region (1), an initial charge will have already been placed on the
capacitor and its value can be roughly estimated from the relation,

$$\bar{V}_o = E_o = \frac{\bar{I}}{\omega c} = \text{constant.} \tag{26}$$

$\bar{I}$ is the half-cycle average current necessary to establish the coercive
force and $\bar{V}_o$ is the half-cycle average capacitor voltage.

If sinusoidal operation (predominant fundamental component of current) is assumed to exist in region (1), then by combining (26) with (25) the low current jump point can be approximated from:

$$E = \frac{(E_s + E_o)(X_L - X_c)}{X_L} = E_o + E_s - I_s X_c. \qquad (27)$$

For the response curves of Fig. MRI-12501 for Hypernik V

$$E_o + E_L > IX_c$$

for all values of C. Note that as C approaches infinity, E approaches $E_s$. This is not the case for all the core materials of the type just discussed. The jump points for the circuit containing an Orthonik core are located on both sides of the limit jump point, Fig. MRI-12502.

In summarizing, it is seen that the initial region of low permeability causes a charge on the capacitor which subtracts from the voltage integral being supplied to the reactor in region (1).

A question might arise concerning the shape of the response curves for 0.5 and 1.0 μμf of Fig. MRI-12501 between values of applied voltage from 37.5v. to 41.5v. and from 15.2v. to 31v. respectively. The current waveforms of supporting harmonic oscillations. A separate section is devoted to the discussion of the oscillations encountered during the course of experimental investigation of the series circuit.

### 4.   Modes of Series Circuit Operation Other Than Ferroresonance.

When dealing with the simple series circuit in connection with the phenomena of ferroresonance, either one of two modes of operation is possible. When operating in the low current region, the current waveform is usually fairly sinusoidal for small values of applied voltage. As the applied voltage approaches the value necessary for occurrence of the ferroresonant current jump, the third harmonic component increases such that the current waveform appears as shown in Fig. MRI-12503-a. When rectangular B-H loop materials are used, the low current waveform ususlly is a square wave; this is due solely to the initial approximate zero slope of the mean magnetization curve.

Once the characteristic ferroresonant current jump occurs, operation takes place in the high current region where the current waveform exhibits a pulse shaped characteristic as illustrated in Fig. MRI-12503-b. The harmonic content of the wave depends upon the sensitivity of the reactor core materials used. When the circuit resistance is small and highly sensi-

tive core materials are used, a steep current pulse is formed and the capacitor voltage waveform approaches a square wave, fig. MRI-12503-c.

Other modes of circuit operation are possible which apparently are independent of the ferroresonant phenomena. These modes occur only for small values of resistance and under certain conditions appear as subharmonic oscillations.

Some experimental work and, to a lesser degree, analytical investigations have been undertaken to determine the factors which cause the subharmonics and the regions in which they can be expected to occur.

In general the regions of oscillations are characterized by increased current magnitudes and waveshapes of unusual form. A difference of opinion exists throughout the literature as to the initial circuit conditions necessary to provoke the oscillations. Experimental work by Rouelle[2], Weygandt and Travis[5], McCrumm[6], and Dehors[7] show that either an initial charge on the series circuit capacitor or an initial flux in the reactor will make possible the oscillations. Analytical proof has also been offered by Weygandt and Travis, and Dehors. Furthermore, Weygandt and Travis, Dehors, and Rudenberg[8] offer analytical proof that the switchingangle of the applied voltage will determine the form of the steady-state responses. However, Weber[4] maintains that the switching angle plays no part whatsoever, his contention being that relay circuit operation using the principles of ferroresonance should then be unpredictable.

In working with low permeability materials, McCrumm observed oscillations in both the low and high current regions. The types of oscillations observed were either sustained and stable, or sustained and unstable (no definite order). He arrived at the conclusion that the high current region of ferroresonance is not subharmonic in nature. More significantly he states that, "Experiment proves that in no case is it possible to induce a subharmonic response by impressing the voltage at an unsuitable high or low value and then gradually bringing the voltage into the range capable of supporting oscillations for the given parameters. This merely results in a high or low current of ferroresonance." In other words, some form of shock excitation is required to produce the oscillations.

---

[5] Subharmonics in Circuits Containing Iron-Cored Inductors, I.A. Travis, C.H. Weygandt, *AIEE Trans.*, 57, pp. 423-30, (1938).

[6] An Experimental Investigation of Subharmonic Currents, J.D. McCrumm, *AIEE Trans.*, 60, p. 538 (1941).

[7] Recherches sur la demultiplication de frequence ferromagnetique, M. Dehors, *Revue Generale de l'Electricite*, Nov. 1947, pp. 455-67.

[8] Non-Harmonic Oscillations as Caused by Magnetic Saturation, R. Rudenberg, *AIEE Trans.*, 68, pp. 676-85, (1949).

Dehors worked with the more rectangular loop materials such as permalloy. The significant results of his work are that two regions of subharmonics were noted. One occurred for very small values of applied voltage where in general the oscillations did not occur spontaneously. The second region was also located in the low current region near the ferroresonant current jump point. No mention was made of subharmonics produced in the high current region. The effective value of the current at the high critical voltages was much smaller than at the low critical voltages. Dehors concluded that when using "ideal" materials, subharmonic oscillations are more difficult to maintain, occur only for small ranges of applied voltage, and appear more often as odd harmonics than even.

During the course of our experimental investigation of the characteristics of the series circuit, various subharmonic responses were encountered. The significant results observed are as follows.

By slowly increasing the applied voltage it was possible to excite a subharmonic oscillation of order three for values of applied voltage which were slightly less than that necessary to cause the ferroresonant jump into the high current region, as shown in fig. MRI-12504-a. In certain cases, the oscillation would disappear just prior to the occurence of the jump point. It is interesting to note that the oscillation occuring in this region was stable, sustained and reproducible. Also circuit operation extended into the region of saturation as can be deduced from the current pulse waveforms and increased magnitude or readily seen from the B-H characteristic of the circuit, fig. MRI-12504-b.

The series circuit also showed a tendency to break into oscillation at the point of return to the low current region, assuming that initial operation was in the high current region. However, a sustained oscillation was never obtained at this point.

No oscillations were observed for very low values of applied voltage in the simple series circuit; however, when an initial core flux was introduced by means of an auxiliary d-c bias winding, oscillations were encountered, thus confirming Dehors' work. More will be stated about these oscillations in the section on the use of the series circuit as an amplifier.

When circuit operation extended far into the region of saturation (high current region) subharmonic responses were always obtained either by slowly increasing the applied voltage until this region was encountered, or by initially energizing the circuit with these same high voltages. Subharmonic currents of orders one, two and three respectively occur for increasing values of applied voltage. In general all current oscillations in the high current region with the exception of order one are unsymmetrical. See figs. MRI-12504-c,d. Fig. MRI-12505-a shows the order one mode which is most common. It was rarely possible to excite an unsymmetrical order one mode indicated in fig. MRI-12505-b. In the regions between the orders one, two, and three unsymmetrical and random (having no definite order) pulse responses were obtained. The typical order two and three modes encountered are shown in figs. MRI-125-5-c,d.

In conclusion, fig. MRI-12505-e illustrates the various subharmonic regions encountered. It appears that in the case of the more sensitive materials, the high current region is most susceptible to subharmonic oscillations; this is contradictory to McCrumm's work. No shock excitation such as initial core flux or capacitor charge is necessary to provoke these subharmonic responses. Although the switching angle of the applied voltage apparently in part determines the steady-state form of the subharmonics, these oscillations are located such that they do not encompass the region of ferroresonance, thereby allowing the successful use of these circuits in relay applications. The results shown were consistently observed for Deltamax, HypernikV, and Orthonik core materials.

## 5. Use of the Series Ferroresonant Circuit as an Amplifier.

This chapter deals with an experimental investigation of the series ferroresonant circuit for possible use as a magnetic amplifier. The present commonly used high gain magnetic amplifier circuits contain dry-disc rectifier units which are the prime cause of unpredictable variations in the circuit responses. The rectifier cell performance suffers from leakage, aging, etc. Effects which in turn are highly dependent upon temperature, rectifier voltage, etc. Thus in certain magnetic amplifier applications where the constancy of error in performance determines the value of the system, such as in precision measuring instruments, it would be highly advantageous to incorporate amplifiers which do not contain rectifier units.

## a) Single Core Circuits.

The simplest saturable reactor circuit possessing a signal control winding is illustrated in fig. MRI-12506-a. By varying the amount of control current which is ordinarily of much lower frequency that the controlled or load current frequency, the degree of core saturation is changed, thereby causing a change in the magnitude of the load current. Considering only the case of a direct current control signal, the addition of direct current bias ampere-turns to the reactor causes a shift to the right of the reactor volt-ampere characteristic for increasing amounts of control bias as indicated in fig. MRI-12506-b.

In replotting the reactor volt-ampere curves of fig. MRI-12506-b, using the load source voltage as a parameter, the transfer characteristic of fig. MRI-12507 is obtained. It is seen that the simple reactor circuit can be used as a linear amplifier within a specified control current range, where the current gain would be determined by the slope of the transfer curve. Although the simple reactor circuit will make possible current and power gain, there will not be an ampere-turn gain. Furthermore it should be remembered that even though the transfer curve is linear, the output waveform depends entirely upon the degree of core saturation.

The single core reactor circuit is limited in use partially by the long time responses associated with it. The use of a large choke in the control circuit in order to constrain the induced harmonic current flow is the main reason for the long time response. Inserting resistance in the control circuit improves the time response; however, the power gain is necessarily reduced because of the increased power demands upon the control source to produce a specified output.

When capacitance is added to the load mesh as in fig. MRI-12508-a, the resultant circuit is of the series ferroresonant type with an added control or bias winding. By means of the graphical method of solution it is possible to predict the circuit behavior qualitatively. The volt-ampere circuit response curves may be single, double or triple valued depending upon the choice of circuit parameters and the degree of core presaturation.

A few examples of the types of response which may be expected are shown in fig. MRI-12508-b.

Referring to the ferroresonant circuit of fig. MRI-12508-a, it was experimentally determined that three different modes of operation are possible depending upon the choice of circuit parameters. Only one mode possessed usable amplifier characteristics which showed an improvement in current gain and time response when compared with the simple saturable reactor circuit.

For a specified set of parameters and values of applied voltage ranging from zero to a critical value $E_o$, the response characteristic of the series circuit assumed the form shown in fig. MRI-12509. Over the linear portion of the characteristic, the current waveform appeared to be fairly sinusoidal, because the circuit operation extended only over the regions of initial and high permeability of the reactor B-H curve. The series circuit was able to provide a maximum current gain six times that of the simple reactor circuit. The magnitude of the usable portion of the transfer curve increased with increasing values of capacitance, a maximum limit occuring when the single response loop ceased to exist. Increasing the load resistance from 0 to 1000 ohms had little effect on the circuit operation. A sudden decrease in current occurred as the bias current was increased and the circuit became unsuitable as an amplifier for larger values of bias current. Referring to fig. MRI-12509, the region of the transfer curve for bias currents greater than 32 ma. were subject to subharmonic oscillations. However for $E$  $E_o$ it was possible to maintain control over the entire transfer characteristic and eliminate the subharmonic oscillations and output current discontinuities. However, the amplifier gain was reduced.

The transient response of the ferroresonant amplifier (MRI-12510-a) to a step input control signal was obtained over the useful region of the transfer curve. By decreasing the circuit capacitance, an improvement in time response was noticed. Transient data was also obtained for the simple reactor circuit amplifier ( fig. MRI-12510-b).

The response time was determined on the basis of the circuit response to 63% of the final magnitude.

In conclusion it is seen that the series circuit amplifier can be made to a higher current gain and a shorter time response than the simple reactor circuit amplifier; however, the range of operation will be much smaller.

When the load mesh voltage is increased above $E_o$, assuming the circuit resistance and capacitance remain constant, the circuit response changes to that of Fig. MRI-12511. This amplifier characteristic is also more sensitive than the simple reactor circuit, but over a very limited range of control current. It possesses a number of serious drawbacks. Upon increasing the control current, the load current suddenly jumps to a large value. However, it is no longer possible to cause a return to the initial low current region by reducing the control bias or changing its polarity. The applied voltage must be reduced instead. This is analogous to a grid-controlled thyratron vacuum tube circuit. Once the thyratron fires, the grid loses complete control, and only a reduction in the plate circuit voltage will allow restoration of the initial conditions.

As the applied voltage was increased towards the normal reactor saturation voltage, the initial load current jump point occurred at a lower control current, thereby causing a reduction in the range of the circuit operation as an amplifier. Also subharmonic oscillations were more prevalent under this circuit operation than in the previously discussed case.

For values of load circuit voltage greater than the saturation value, it was possible to increase the load resistance until the ferroresonant current jump and hystersis phenomena were eliminated. The resultant transfer characteristic is plotted in Fig. MRI-12512.

## b) Double Core Circuits.

By using two reactors as illustrated in Figs. MRI-12513-a and MRI-12517-a, it is possible to eliminate the control choke. The odd harmonics cancel but a second harmonic circulates in the control circuit. The transfer curve for this circuit when operating at low values of load voltage is plotted in Fig. MRI-12513-b.

When capacitance is added to the load mesh, the circuit again becomes a biased ferroresonant network. The transfer curves taken for C = 2μf, 3μf are also shown in Fig. MRI-12513-b and it is seen that the introduction of capacitance does provide regions of gain greater than that of the double-core reactor circuit. Also the low voltage transfer curve allows an increase or decrease in load current for increasing bias depending upon the region of operation. Unlike the transfer curves for the single core ferroresonant amplifier, the region of low bias currents extending to the load current maximum was

very prone to oscillate at subharmonic frequencies. Referring to the transfer
curve taken for C = 3μf the load current waveform remained fairly sinusoidal
until the bias current reached 18 ma. The change in slope of the transfer
curve at this point was accompanied by an initiation of subharmonic oscillations,
the region of which extended to a bias current of 35 ma. The load current
then became peaked, corresponding to the usual high current region waveform of
ferroresonant circuits. For extremely large bias currents, the transfer curve
approached a horizontal asymptote corresponding to complete core saturation.

Considering first the region of subharmonic oscillations, it was
determined that a simultaneous variation of load resistance and capacitance,
and control bias was necessary to produce the subharmonic waveform and fre-
quency desired. The value of control circuit resistance was not too im-
portant, whereas the number of control ampere-turns was important. Also,
an increase in load resistance and capacitance caused an increase in fre-
quency. Fig. MRI-12514-c illustrates a 3.5 cycle per second oscillation
having excellent sinusoidal waveform and stability. The 60 cycle carrier
can also be modulated more than 100% resulting in the waveform of fig. MRI-
12514-d. A possible application for this mode of operation would be a square
wave oscillator or a low frequency multivibrator.

The usable range of circuit operation for low applied voltages is
over that part of the transfer curve which shows a decrease in load current
for an increase in control current. Referring to fig. MRI-12513, when a
3μf series capacitor is used, the circuit would normally be operated between
38 and 48 ma. The transient responses of the simple reactor and ferro-
resonant circuits over this range are shown in fig. MRI-12517-a,b. In this
case there was an apparent increase in time response due to the addition of
the capacitance to the double-core reactor circuit. Decreasing the cap-
acitance tended to further peak the response curve, and further increase
the gain over the usable region already mentioned. However, a limit was
reached when the current became discontinuous over the working range. For
the 2μf characteristic of fig. MRI-12513, the ferroresonant amplifier po-
ssesses a gain which is ten times greater than the most sensitive region of
the double-core reactor circuit.

Proceeding to the operation of the double core ferroresonant circuit
at high voltages, it was noted that the circuit would oscillate very easily
at low values of control current. The load resistance was increased until
these oscillations entirely disappeared. However, the resulting circuit re-
sponses did not exhibit any worthwhile amplification regions at the high val-
ues of applied voltage and so further investigation was abandoned.

By completely constraining harmonic flow in the control circuit
by the addition of a shoke, the circuit transfer curves closely resembled the
volt-ampere response curves of the simple ferroresonant series circuit except
for increased subharmonic responses. By increasing the load resistance to the
critical value of 800 ohms, load current jumps and hysteresis effects were
eliminated, and the single-valued transfer curve of fig. MRI-12515 was ob-

tained.  This characteristic was not obtainable if the control choke was removed.  Over the most sensitive part of this curve, the ferroresonant amplifier exhibited a larger current gain than the double-reactor circuit by a factor of ten.  The transient responses of both circuits were determined (fig. MRI-12516-a,b) for the sensitive range occurring for control currents ranging from 19-32 ma.  The addition of capacitance appears to have little effect upon the circuit operation.  By changing the load resistance to 230 ohms, the slope of the sensitive region of the ferroresonant amplifier changed little.  However, by referring to figs. MRI-12516-b,c, it is observed that the transient buildup and decay times for the amplifier could be readily equalized if desired.

In conclusion, the constrained double-core series ferroresonant circuit appeared to yield the most favorable amplifier characteristic.  It was not infested with regions of subharmonic oscillations, or current discontinuities.  By using precision components and adjusting the load resistance to the critical value just necessary to eliminate the ferroresonant current jump, amplifier gains much greater than ten can be realized as compared with the double-core reactor circuit.


## 8.    Use of Ferroresonance to Improve Magnetic Amplifier Performance.

The series ferroresonant circuit can be made to perform as an amplifier under certain conditions previously discussed.  In general it is possible to produce amplifier transfer curves which exhibit regions in which the circuit gain is greater than that of the corresponding simple reactor circuit (see figs. MRI-12509 and MRI-12515).  However, there are definite limitations to the extensive use of this type of amplifier.  Referring to fig. MRI-12515 it is seen that the useful control range is limited to a small region of the entire transfer characteristic.  Also the circuit gains obtainable are still low when compared with presently used external feedback or self-saturating magnetic amplifier types.  Finally, in order to obtain the stable high gain regions, one finds that the choice of circuit parameters is quite critical.  Therefore it was decided to explore the possibility of using ferroresonant amplification in conjunction with existing high gain magnetic amplifier circuits in order to obtain greater amplifications.

## a)  External Feedback Circuit.

The commonly used external feedback circuit shown in fig. MRI-12517-b differs from the simple reactor circuit of fig. MRI-12517-a only in that a positive feedback winding energized by the load circuit is used to increase the overall amplification by providing an ampere-turn gain greater than unity.  The notable characteristics of the external feedback circuit are that

a) Higher gains can be achieved as compared with other sensitive amplifier circuits.

b) Feedback can be increased until the transfer curve exhibits binary stability.

c) Rectifier limitations such as temperature and aging effects are not as important as in other type circuits.

The main disadvantage is the necessity of providing core window area for the feedback turns, which automatically results in working the reactor at less than the normal volt-ampere rating.

By placing a capacitor in series with the load circuit parameters, fig. MRI-12517-b, the circuit then becomes one of two types. If the effect of the capacitance is small as compared to the external feedback, then the circuit should be referred to as an external feedback amplifier employing ferroresonance. However, if the ferroresonant effects predominate, then the circuit would properly be referred to as a series ferroresonant amplifier employing external feedback.

In fig. MRI-12518 are plotted the transfer curves of an external feedback circuit. Curve (1) is the normal transfer curve. Curve (2) represents the use of a series capacitance of 5μf. By reducing the value of capacitance, the transfer curve exhibits binary stability. One immediately recognizes the increased gains obtainable without loss of linearity. Also the control range is increased. Transfer Curve (2) has a gain 2.5 times that of the simple external feedback circuit. Also in checking the transient responses over the sensitive gain regions, it was found that the time of response was practically constant. Therefore, an important consideration in the use of ferroresonance is that the gain per cycle figure of merit for for an amplifier is increased.

The transfer curves of a constrained amplifier are given in fig. MRI-12519 and are self-explanatory. Curve (4) possesses a current gain 10 times that of the non-ferroresonant response curve (2). The occurrence of a resonance condition when capacitance is introduced into the circuit is clearly shown by curves 3,4 and 5. As the capacitance is increased, the maximum circuit current passes through an optimum value.

It is well known that supply voltage variations cause a per cent change in the magnetic amplifier gain which is proportional to the change in supply voltage for small variations. Fig. MRI-12520 clearly illustrates this condition. It should be noted that while the transfer curves appear to pivot about a single minimum point, this is only true as long as the symmetrical flux excursion does not extend into the saturation region. In general, the minimum load current will increase with increasing line voltage.

The effect of line voltage variations on an amplifier employing ferroresonance is shown in fig. MRI-12521. An important conclusion is that the per cent change in amplifier gain is no worse than that obtained with the simple external feedback circuit.

In considering the effects of ferroresonance on the external feedback circuit, which will hold for the self-saturating circuits also, one might immediately draw the conclusion that the capacitor is a positive feedback device. However, although the circuit responses appear to substantiate this conclusion, the effect on the physical operation of the circuit is quite different from that of the feedback turns. The feedback ampere-turns provide a bias point for the core from which the flux excursion determined by the magnitude of supply voltage, begins. When capacitance is added, the average core bias remains the same as before. However, the flux excursion is increased since the capacitance aids the supply voltage by supplying additional voltage integral. From experimental observation it is noted that there is also an important difference between the effect of the capacitor and the supply voltage on the minimum point of the transfer curve. Increasing the supply voltage in order to increase the amplifier gain causes a rise in the minimum point, whereas the minimum point remains fixed when capacitance is used, (fig. MRI-12519) and only the circuit gain is altered.

The effect of line frequency variations on circuit performance is of importance especially in connection with the design of amplifier circuits for military equipment. On might expect that the use of ferroresonance would be detrimental to the feedback amplifier operation since the capacitive reactance is a complicated function of frequency. Referring to figs. MRI-12522 and MRI-12523 it is observed that there is little difference in the per cent changes in gain between the simple feedback circuit and the ferroresonant-aided circuit.

The effect of ferroresonance on the operation of a binary stable external feedback amplifier was studied. The important results are shown in fig. MRI-12524. Transfer curve (1) represents a bi-stable feedback amplifier. The circuit response when capacitance is added to the load mesh, is illustrated by curves (2,3). Again the resonant peaking of the load current is obvious. Also it is interesting to note that the initial point of instability is independent of capacitance. Therefore, it is suspected that the core biasing due to the feedback ampere turns is mainly responsible for the location of this point because the initial jump point is a function of the circuit capacitance in the simple series ferroresonant circuit. The principle effect of the capacitance is to increase the limits of the binary region. This may be very useful in certain type switching applications.

b) Self-Saturating Circuits

The self-saturating type magnetic amplifier, one type of which is shown in fig. MRI-12517-o, is important because greater output power can be obtained for the same core size used in an external feedback circuit, since the load and feedback windings are one and the same. The main disadvantages of this type amplifier are that rectifier performance characteristics such as leakage, aging, etc. are detrimental and usually result in a loss of circuit gain. Also the circuit cannot be made unstable unless external feedback turns are added.

The investigation of the effects of ferroresonance on a self-saturating type amplifier is limited to those circuits possessing an a.c. output in order that blocking action by the capacitor does not occur. The doubler circuit was chosen as a typical example. Curve 1 of fig. MRI-12525 is the normal doubler transfer curve, whereas curves (2,3) show the effects of ferroresonance. Note that while the gain of curve 2 is 3 times that of curve 1, the control range is reduced. Curve 3 again illustrates the load current peaking due to resonance phenomena. The amplifier can be made unstable for values of capacitance less than 2 μf.

The core material used in the circuits discussed so far in this section was U-type Hymu 80 laminations. These laminations are usually supplied with a double yoke width in order to decrease local saturation effects. The effect of the air gap is to cause lower gains as compared to a closed magnetic path circuit.

The effect of ferroresonance on the gain of a doubler circuit using a highly sensitive tape wound core of Hypernik V material is seen in fig. MRI-12526. Curves 2 and 3 are of interest because of the slight instability obtained for increasing control bias, whereas decreasing bias produced only a single-value response. Curve 3 also represents the maximum beneficial effects of ferroresonance. Although the gain is slightly increased, the maximum power output has been decreased. The conclusion drawn is that ferroresonant techniques will do little if anything to improve the performance of amplifiers using very sensitive core materials.

Since the U-type lamination is preferred in many designs because of the simpler coil winding and production control techniques, one immediately recognizes the importance of using ferroresonance in conjunction with the feedback and self-saturating type circuits. The gains of these circuits can be made comparable to those of the more expensive circuits employing highly sensitive core materials.

Another consideration for the use of ferroresonant techniques in self-saturating circuits is in connection with the rectifier problem. Resistance shunting of the rectifiers results in a reduction of the effects on the circuit operation of rectifier aging, leakage and changes due to variations in temperature. However, a loss in gain is associated with this compensation. Therefore, by introducing ferroresonance into the circuit it is possible to restore this loss in gain.

During the course of experimentation with the doubler type self-saturating circuit, it was found that moderate capacitance shunting of the circuit rectifiers produced a shift of the transfer curve to the right (see curves 1,2, and 3 of fig. MRI-12527), without noticeable loss in gain. Large shunting capacitance definitely caused serious gain reduction. The great significance of this "shifting" effect is that the necessity of providing bias ampere-turns, to cause minimum load current to occur for zero

control signal, can be entirely eliminated. Curve 2 of fig. MRI-12527 illustrates the reduction of "stand-by" load current without the loss of circuit gain. Curve 3 illustrates maximum reduction with a slight loss in gain. By combining ferroresonance with this phenomena, both a shifting of the transfer curve and an increase in its slope can be effected as shown by curves 4 and 5 of fig. MRI-12527. Thus the ultimate in magnetic amplifier design is approached with relative simple circuitry techniques.

In order to illustrate more significantly the importance of using ferroresonance to improve magnetic amplifier performance, a doubler circuit was constructed using a three-legged reactor (E-I laminations) of low permeability "Transformer C" material. The circuit gain was increased by means of ferroresonance to the point of instability and the transfer data plotted in fig. MRI-12528. The ferroresonant aided doubler exhibits a current gain 20 times that of the simple doubler circuit. This means an increase in power gain of '00. The maximum power output has been greatly increased over the entire usable control range of the simple doubler. Also of particular interest is the fact that the minimum point is not changed by use of ferroresonance.

Although it has been shown that present day amplifier circuit performance can definitely be improved by the careful use of ferroresonance, an exhaustive study of its possibilities has by no means been made. Also, one should be cautioned at the ever present possibility of exciting subharmonic oscillations which are closely related to ferroresonant phenomena.

## List of Symbols

$C$ = Capacitance, farads

$e$ = Instantaneous value of applied voltage, volts

$E$ = R.M.S. " " " " " "

$\bar{E}$ = Half-cycle average value of applied voltage, volts

$E_c$ = Critical " " " " " "

$E_L$ = Reactor voltage, R.M.S., volts

$E_m$ = Maximum value of applied voltage, volts

$E_o$ = Average capacitor voltage due to magnetizing current, volts

$E_s$ = Reactor saturation voltage, volts

$i$ = Instantaneous value of current, amperes

$\bar{I}$ = Average value of magnetizing current for half-cycle, amperes

$i_1$ = Instantaneous current in region 1, amperes

$i_2$ = " " " " " 2, "

$I$ = R.M.S. value of load current, amperes

$\bar{I}$ = Half-cycle average value of current, amperes

$I_1$ = Fundamental R.M.S. component of current, amperes

$I_s$ = Saturation current, amperes

$\bar{I}_2$ = Half-cycle average value of current in region 2 of B-H curve, amperes

$N$ = Turns on load winding

$P$ = Consumed reactor power, watts

$R$ = Total circuit resistance, ohms

$R_c$ = Critical resistance for single valued current jump, ohms

$R_e$ = External circuit resistance, ohms

$R_L$ = Apparent reactor resistance, ohms

$t$ = Time, seconds

$t_1$ = Time of entry into region 1

$t_2$ = " " " " " 2

$v_c$ = Instantaneous capacitor voltage, volts

$V_c$ = Initial magnitude of capacitor voltage upon entry into region 1, volts

$\bar{V}_o$ = Average capacitor voltage due to magnetizing current, volts

$\omega$ = Angular frequency of supply, radians per second

$\omega'$ = Effective angular frequency, " " "

$X$ = Total effective reactance, ohms

$X_c$ = Capacitive reactance, ohms

$X_L$ = Inductive " , ohms

## List of Symbols (Cont'd)

$\theta$ = Phase angle, degrees

$\theta_1$ = Angle of entry into region 1, degrees

$\theta_2$ = " " " " " 2, "

$\psi$ = Core flux, lines

$\psi_s$ = Saturation flux, lines

* = Indicates modification for presence of current harmonics

R     C

$e = E_m \sin \omega t$

(a)

B

H

(b)

B

H

(c)

B

H

(d)
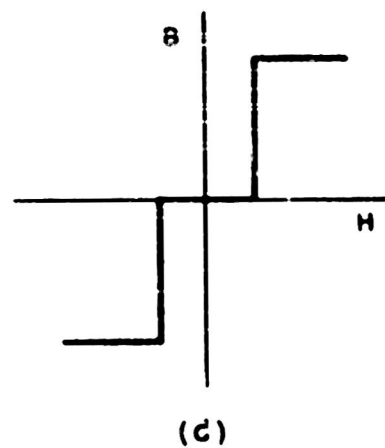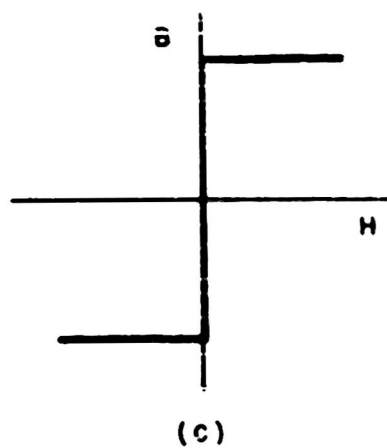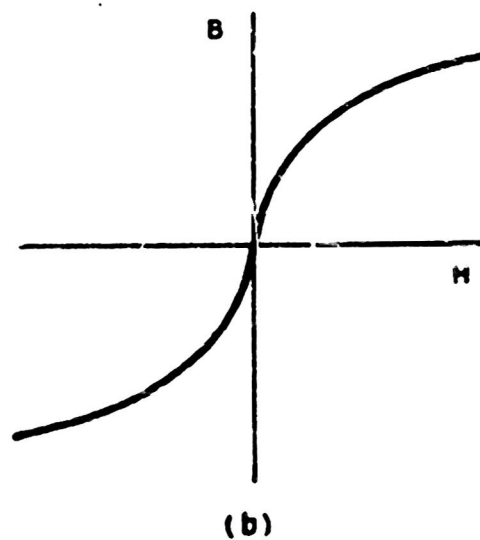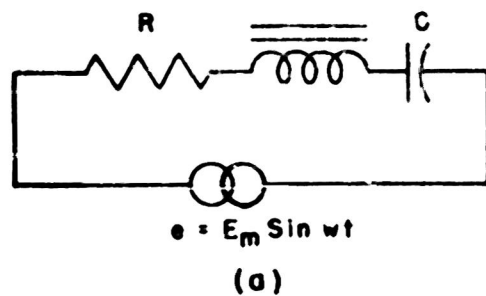
DELTAMX
(e)
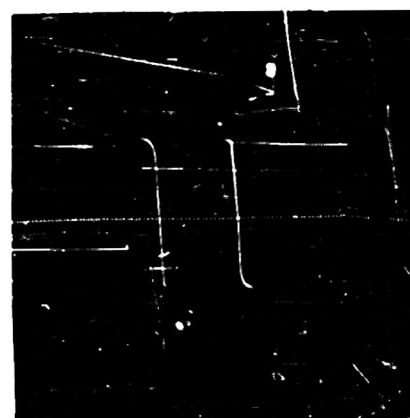
HYPERNIK V
(f)

REACTOR VOLT-AMPERE CHARACTERISTICS

DELTAMAX

HYPERNIK Ⅴ

FIG. 3

E (volts) rms.

I (ma)

(a)



(b)



(d)



(e)
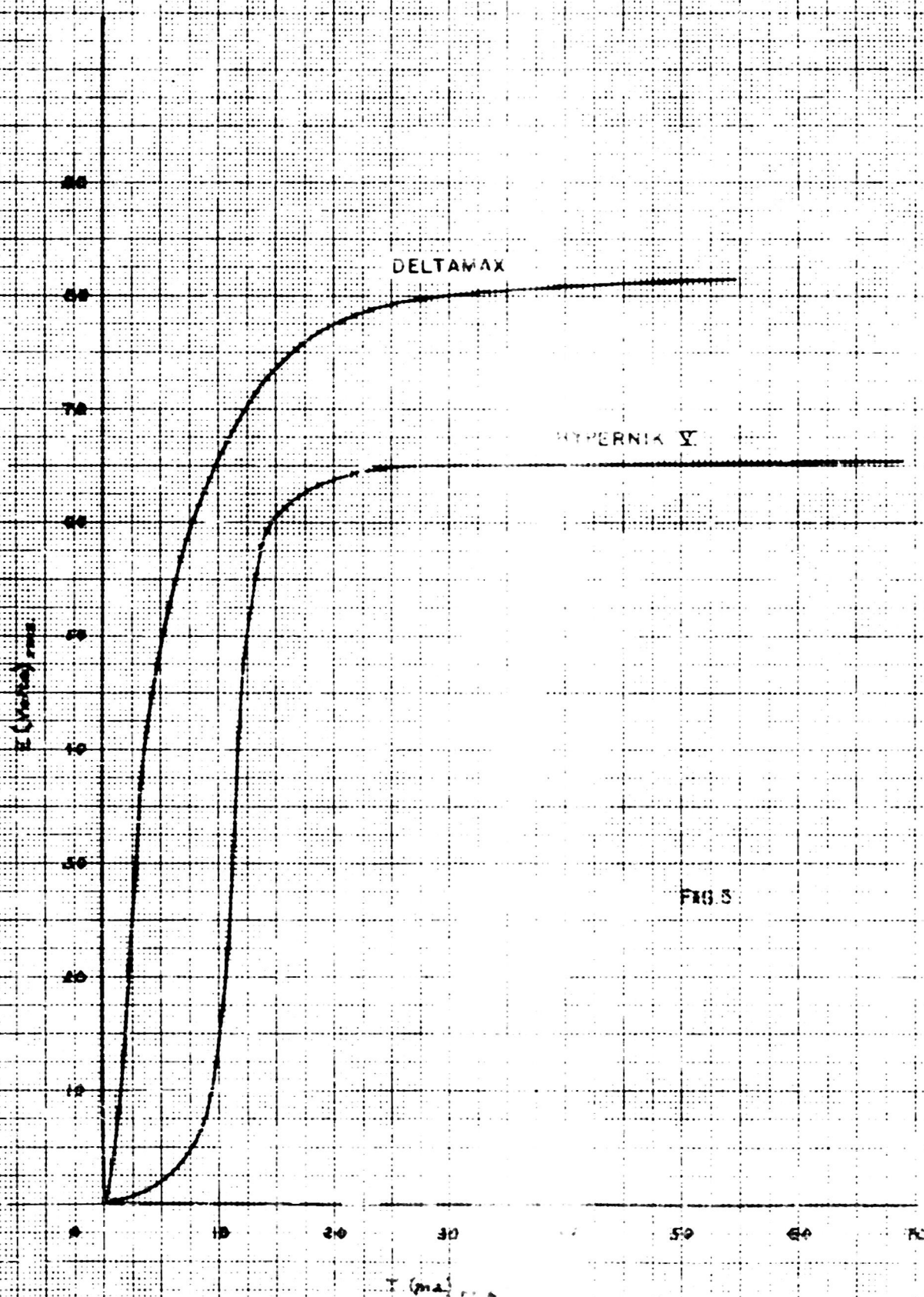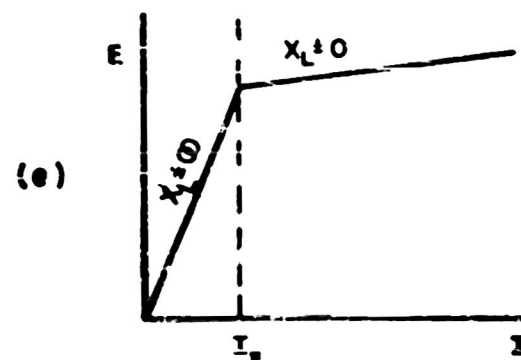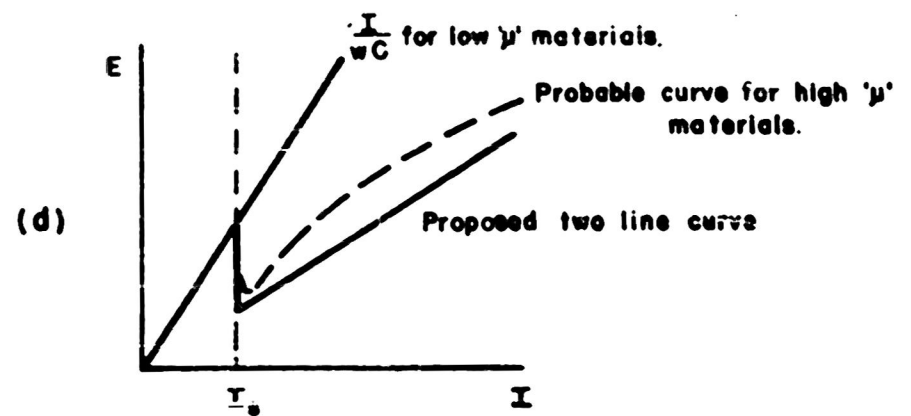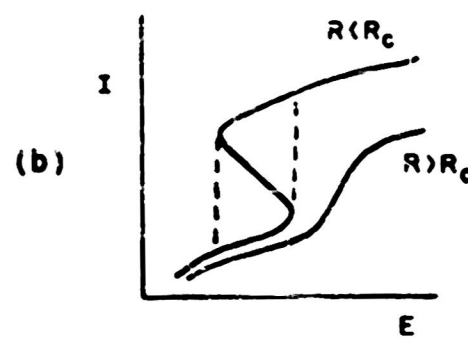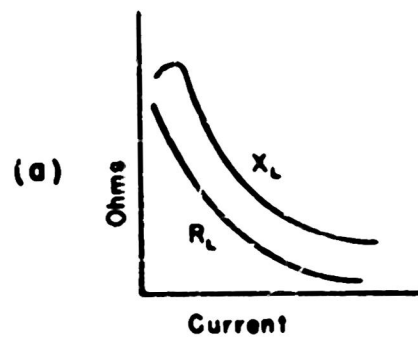
## RESPONSE CURVES FOR THE SERIES FERRORESONANT CIRCUIT
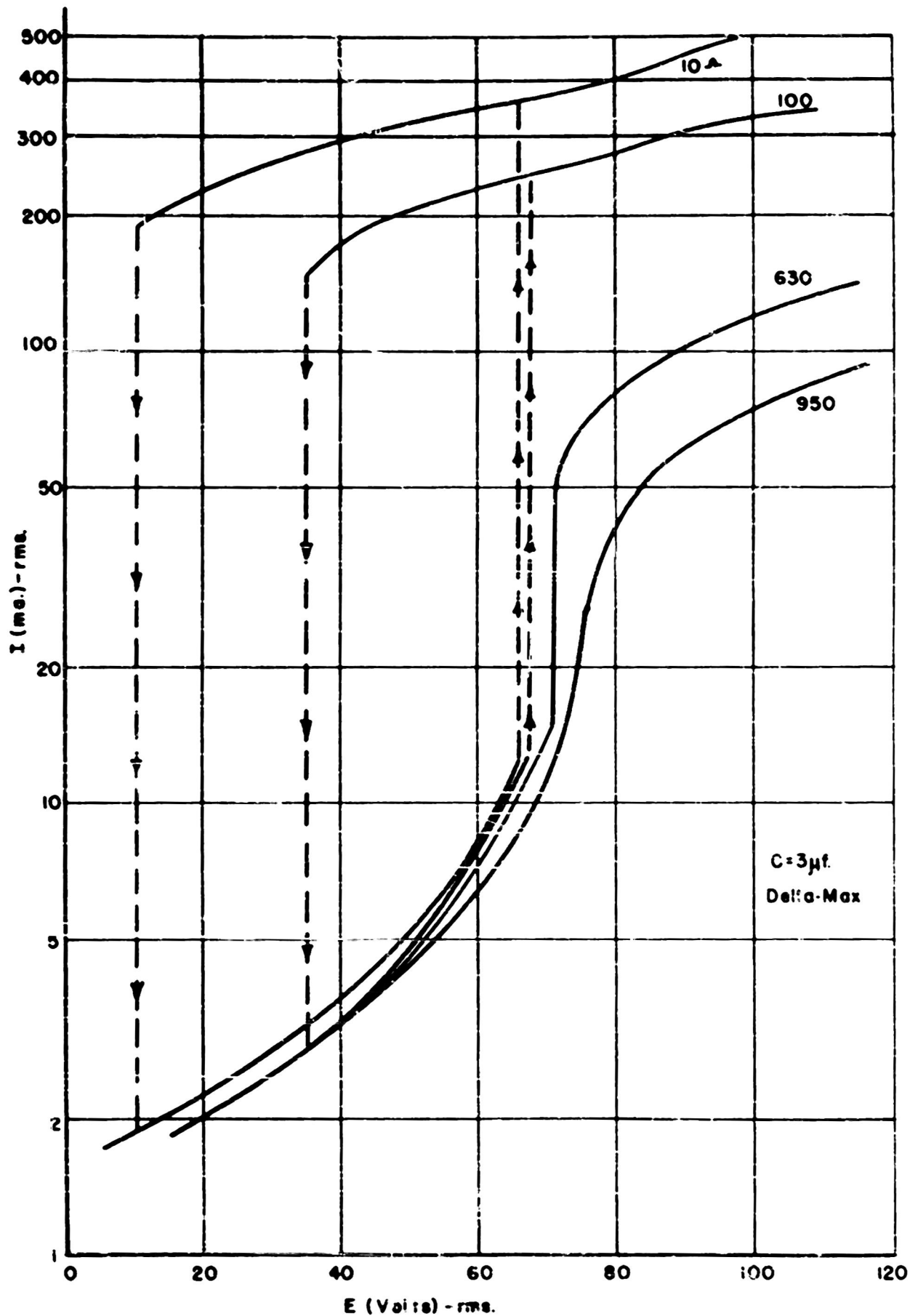


$C = 3\mu f.$

Delta-Max

I (ma.) - rms.

E (Volts) - rms.

M.R.I.-12487

CURRENT HARMONICS ASSOCIATED WITH DELTAS A

GRAPHICAL SOLUTION OF THE SERIES FERRORESONANT CIRCUIT

Voltage

Current-Ma.

C=.77 µf.

C=1.54

C=2.07

R=667 Ω

$\frac{I}{wC}$

$\frac{E}{R}$

M.R.I.-12490
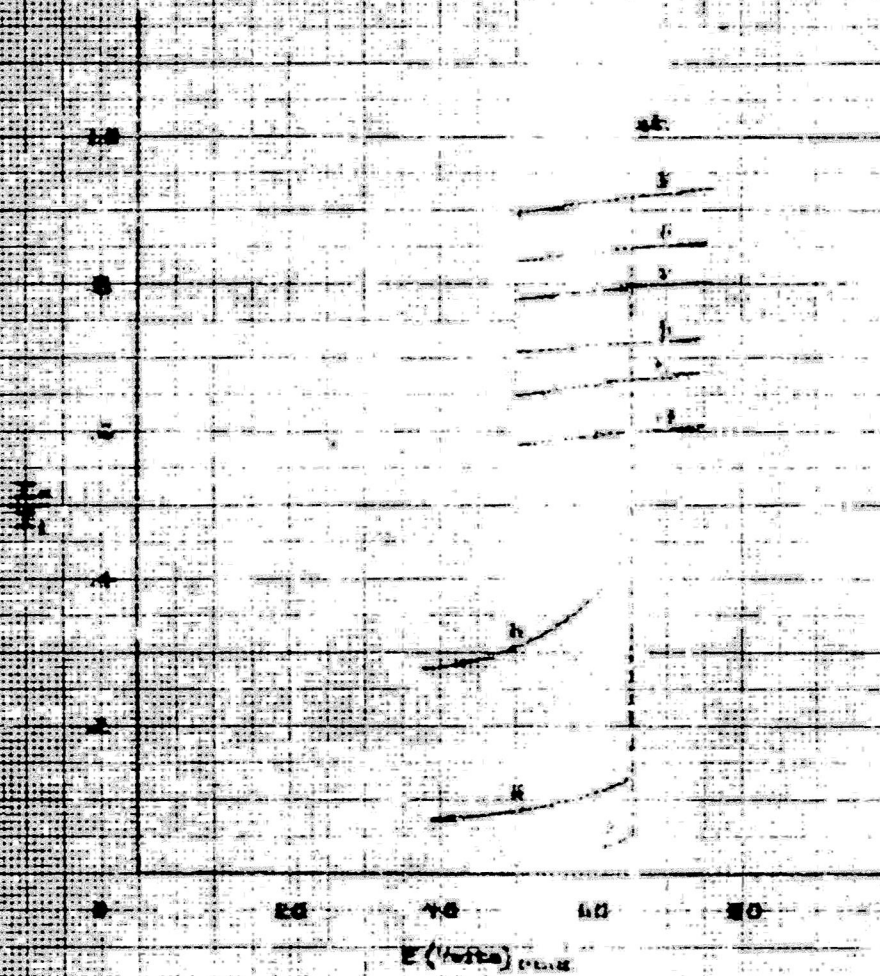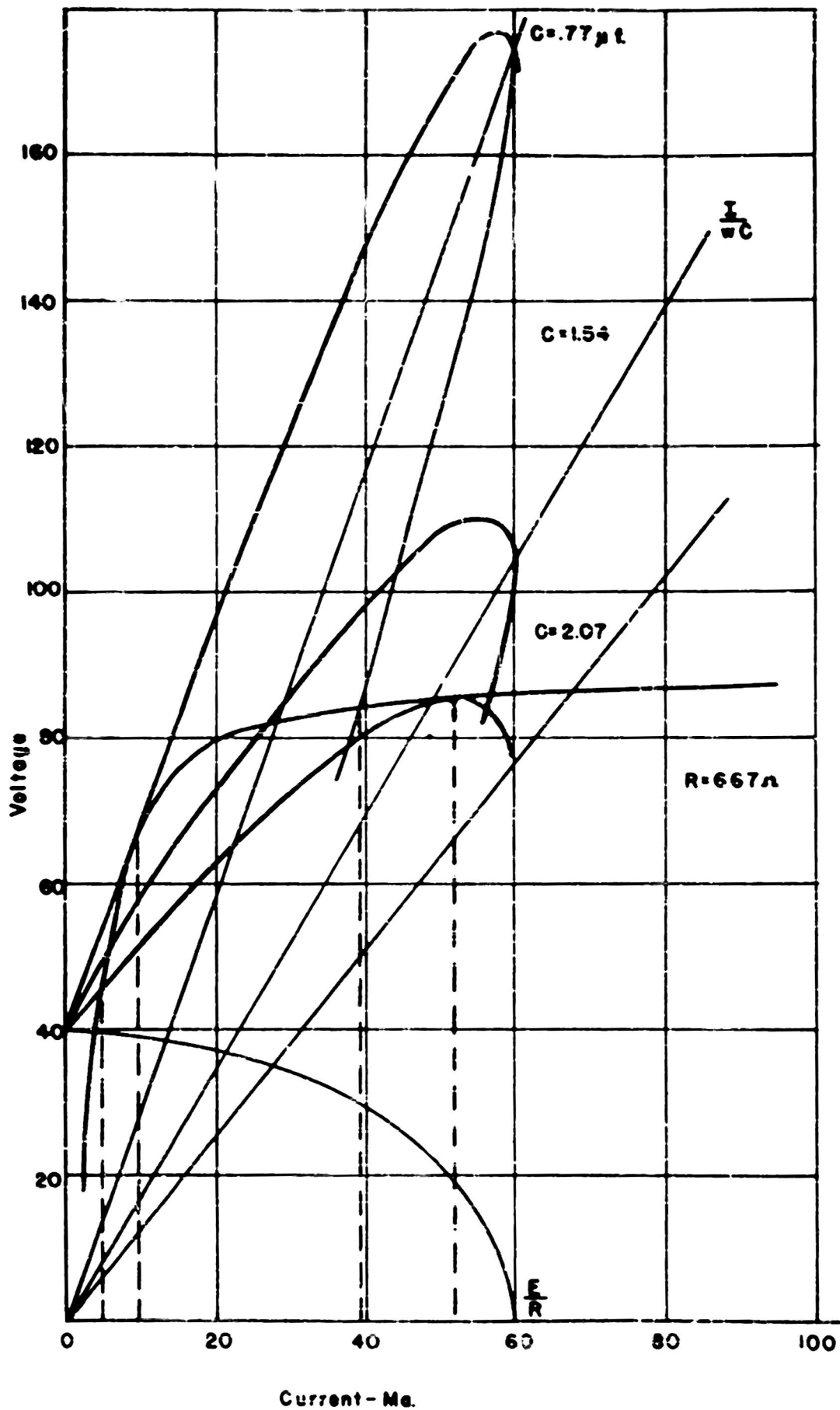
# RESPONSE OF THE SERIES FERRORESONANT CIRCUIT AS A
## FUNCTION OF CAPACITANCE

100

50

20

Current - Ma.

Calculated

10

5

Experimental

2

1

0          1          2          3          4

Capacitance - μf.
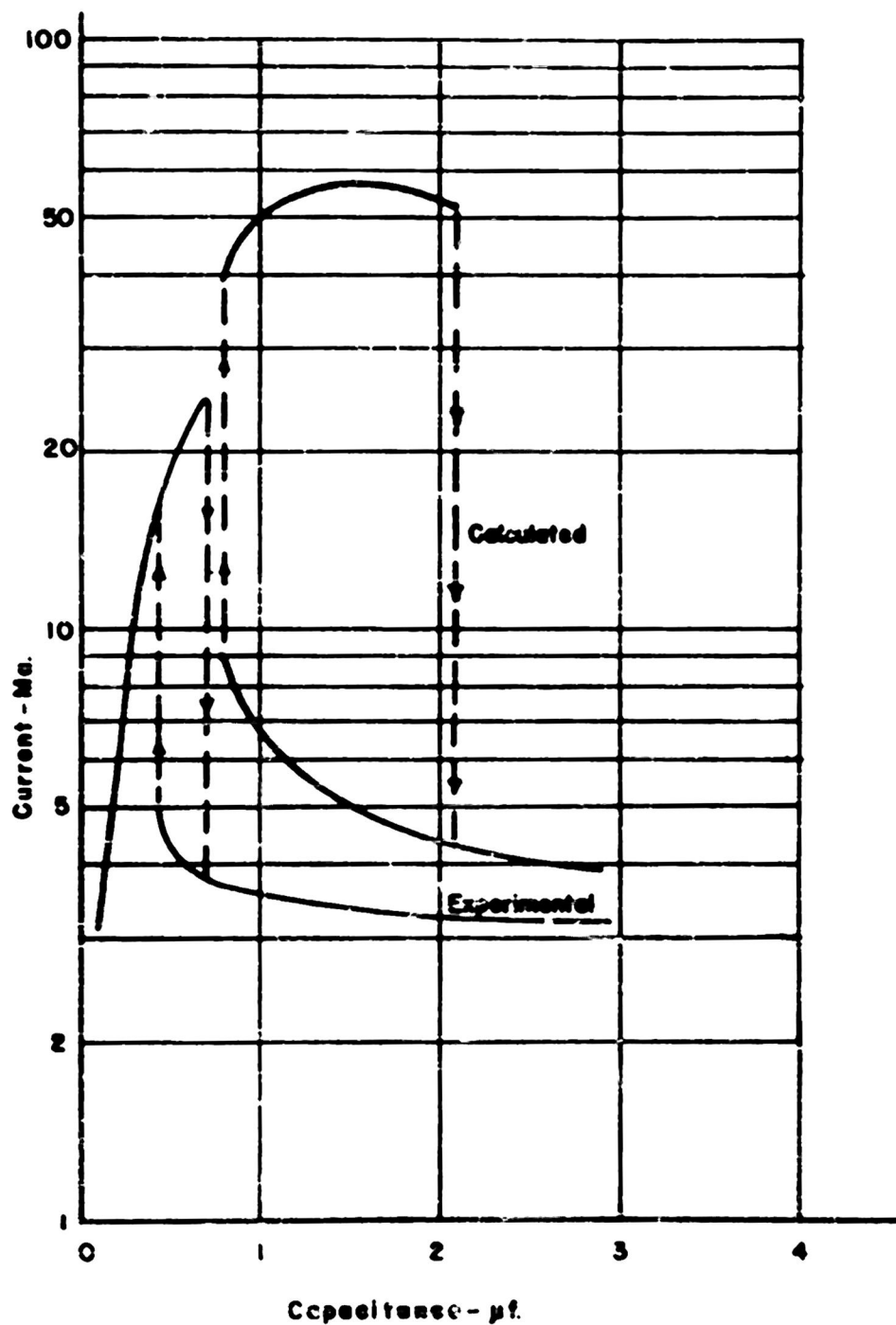
# GRAPHICAL SOLUTION OF THE SERIES FERRORESONANT CIRCUIT

### ( Method of Odessey & Weber )



Current — ma.

Voltage

M.R.I. - 12492
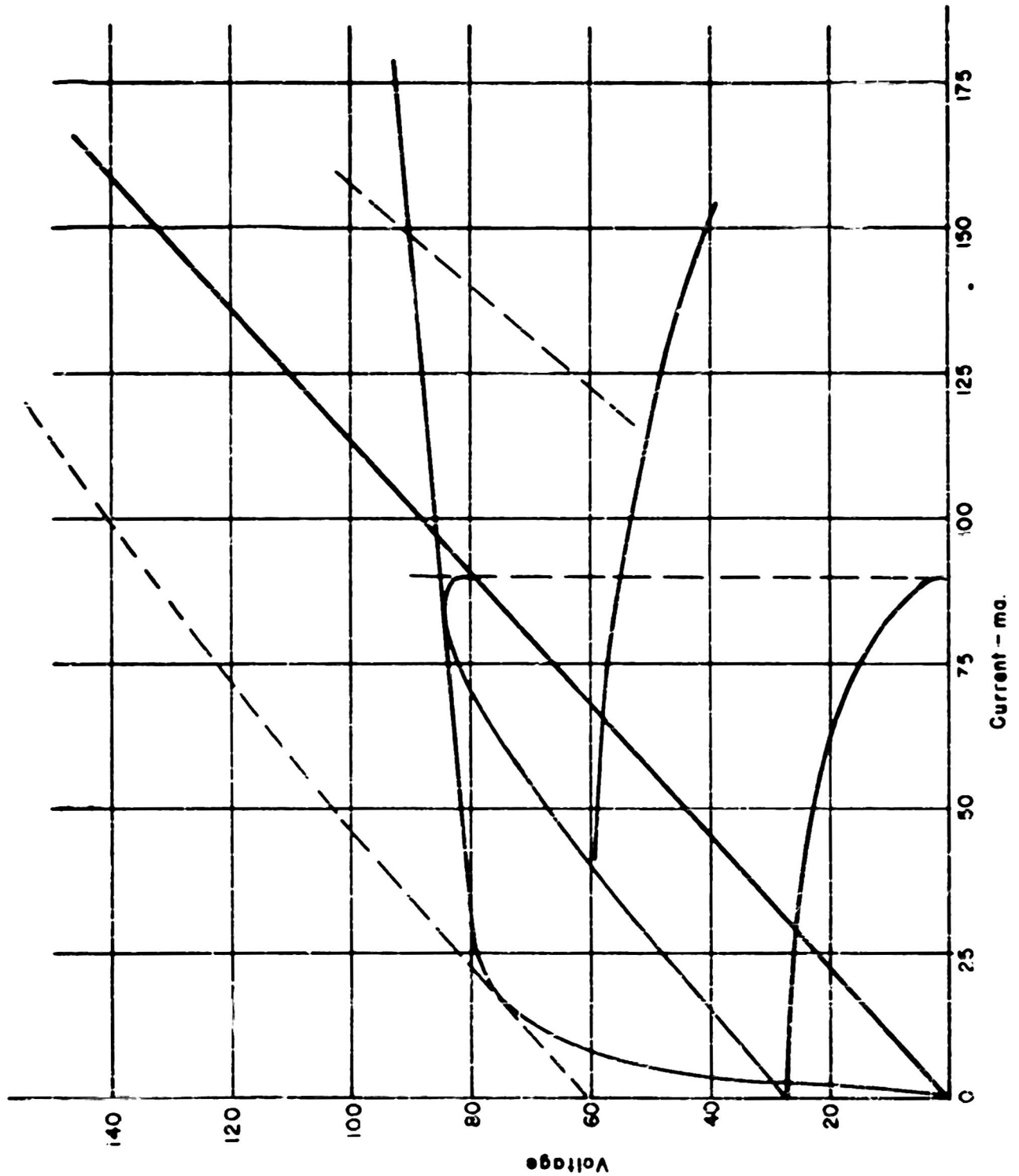
GRAPHICAL SOLUTION OF THE SERIES FERRORESONANT CIRCUIT

(Modification of Odessey & Wuber Method)
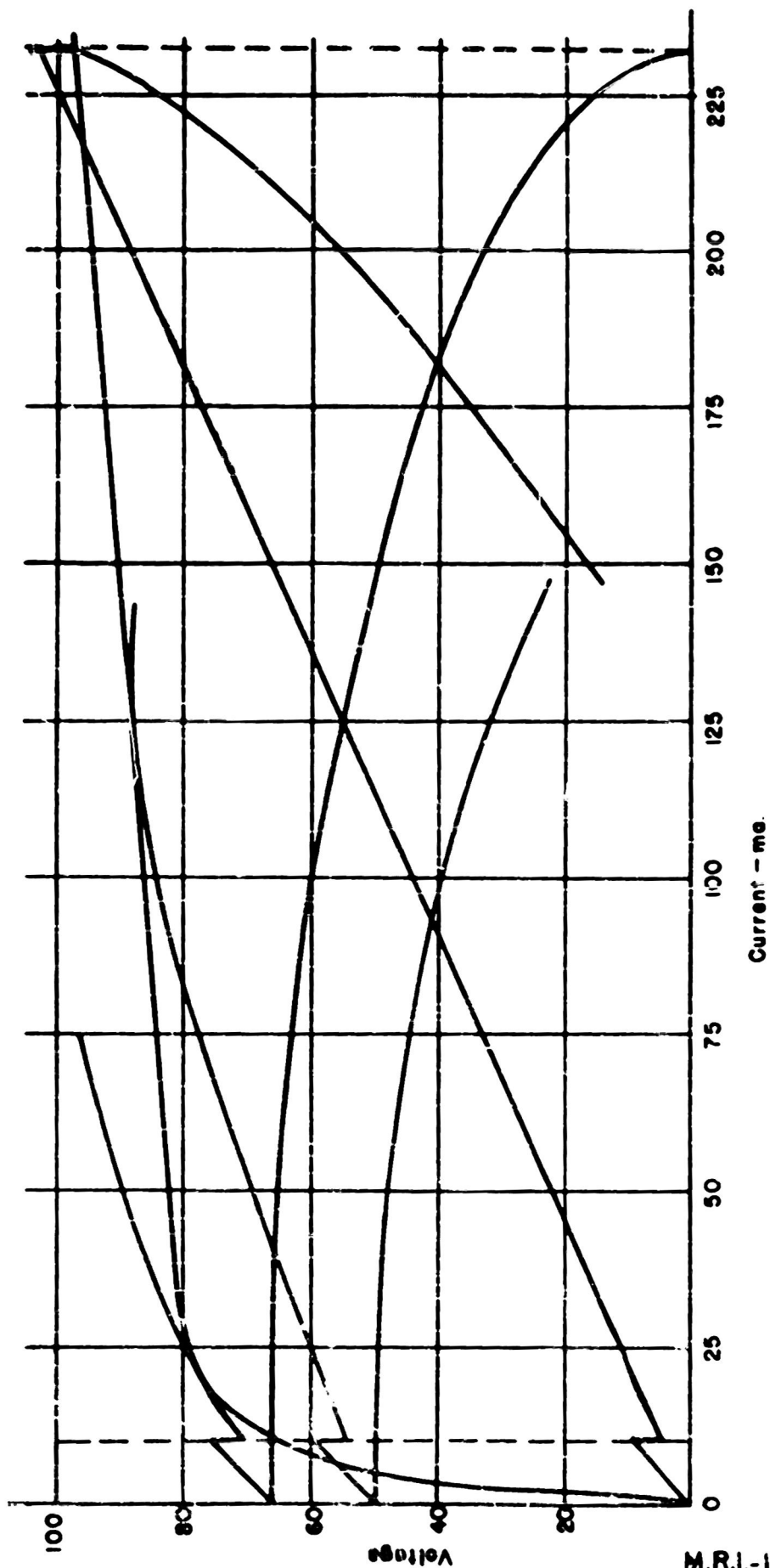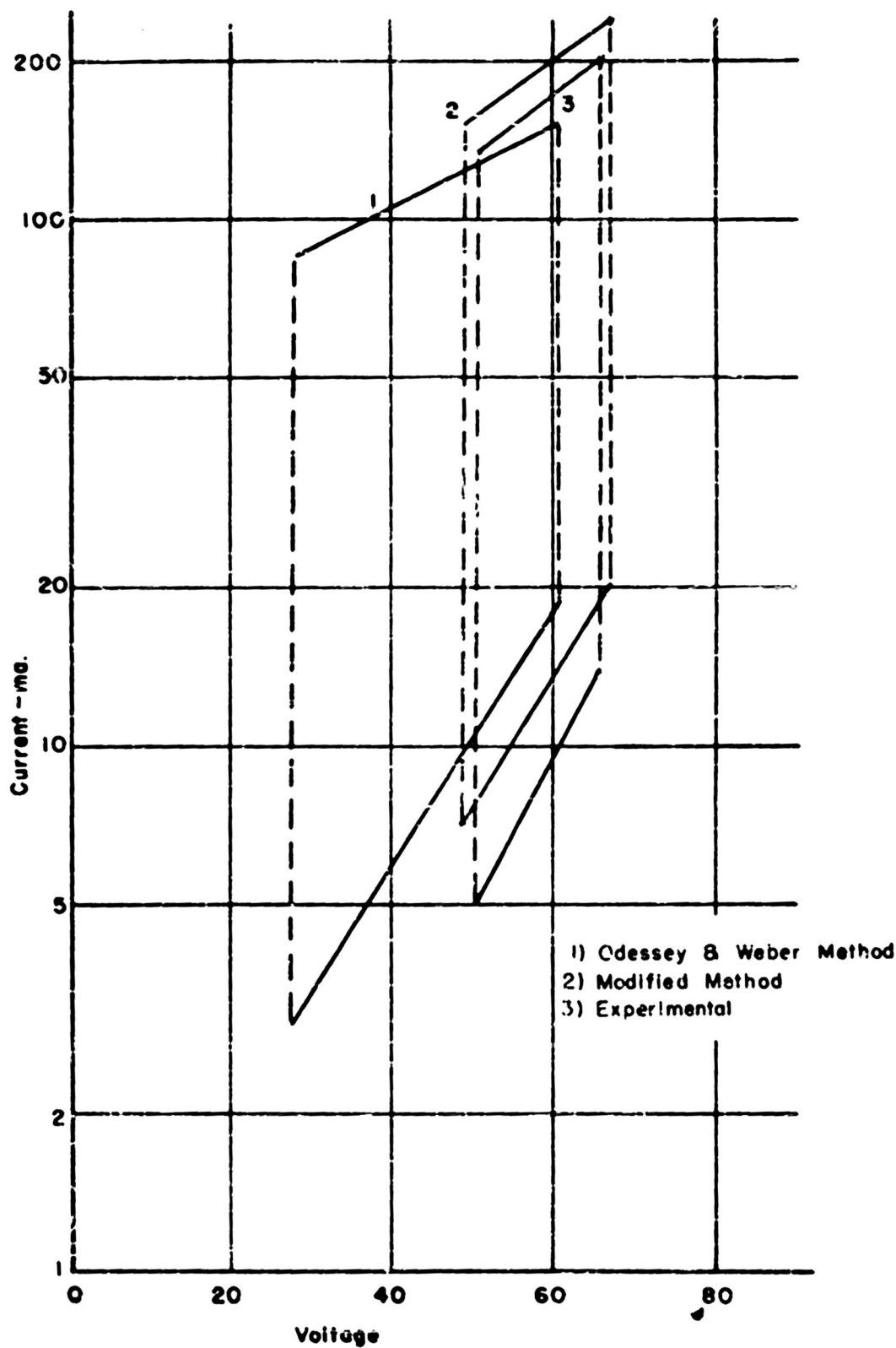
Current — ma.

Voltage

M.R.I.-12493

RESPONSE OF THE SERIES CIRCUIT

1) Odessey & Weber Method
2) Modified Method
3) Experimental

*Current - ma.* (y-axis)

*Voltage* (x-axis)

(a)

(b)

(c)

(d)

Increasing RC

# AVERAGE VOLT-AMPERE RESPONSE OF THE SERIES CIRCUIT



Deltamax Core
C = 3 µf.
1) R = 15 Ohms
2) "   100  "
3) "   200  "
4) "   700  "

# AVERAGE VOLT-AMPERE RESPONSE OF THE SERIES CIRCUIT



Deltamax Core
R = 200 Ohms
1) .15 μf.    4) 5 μf.
2) 1 "       5) 8 "
3) 3 "

Current — ma.

Voltage
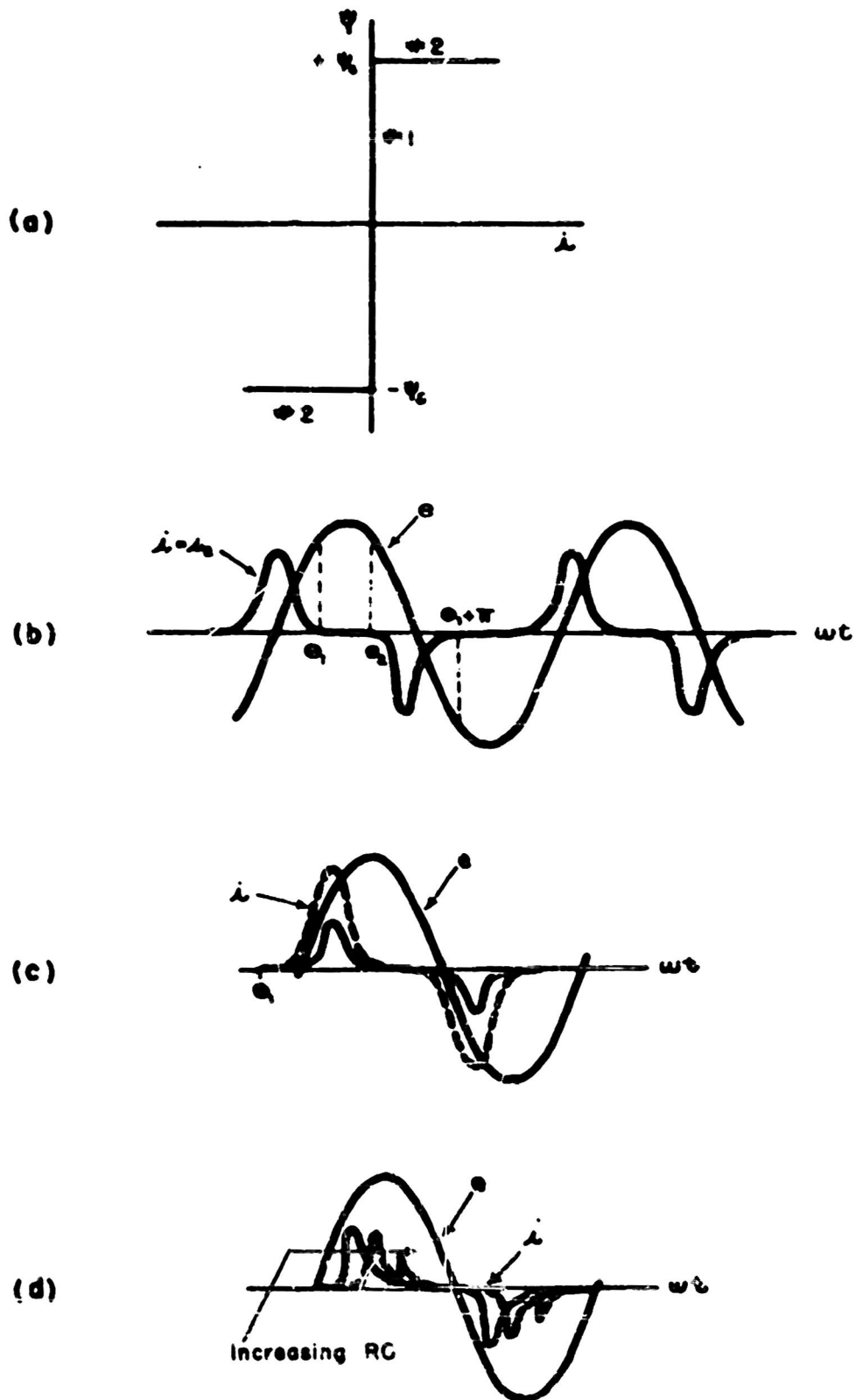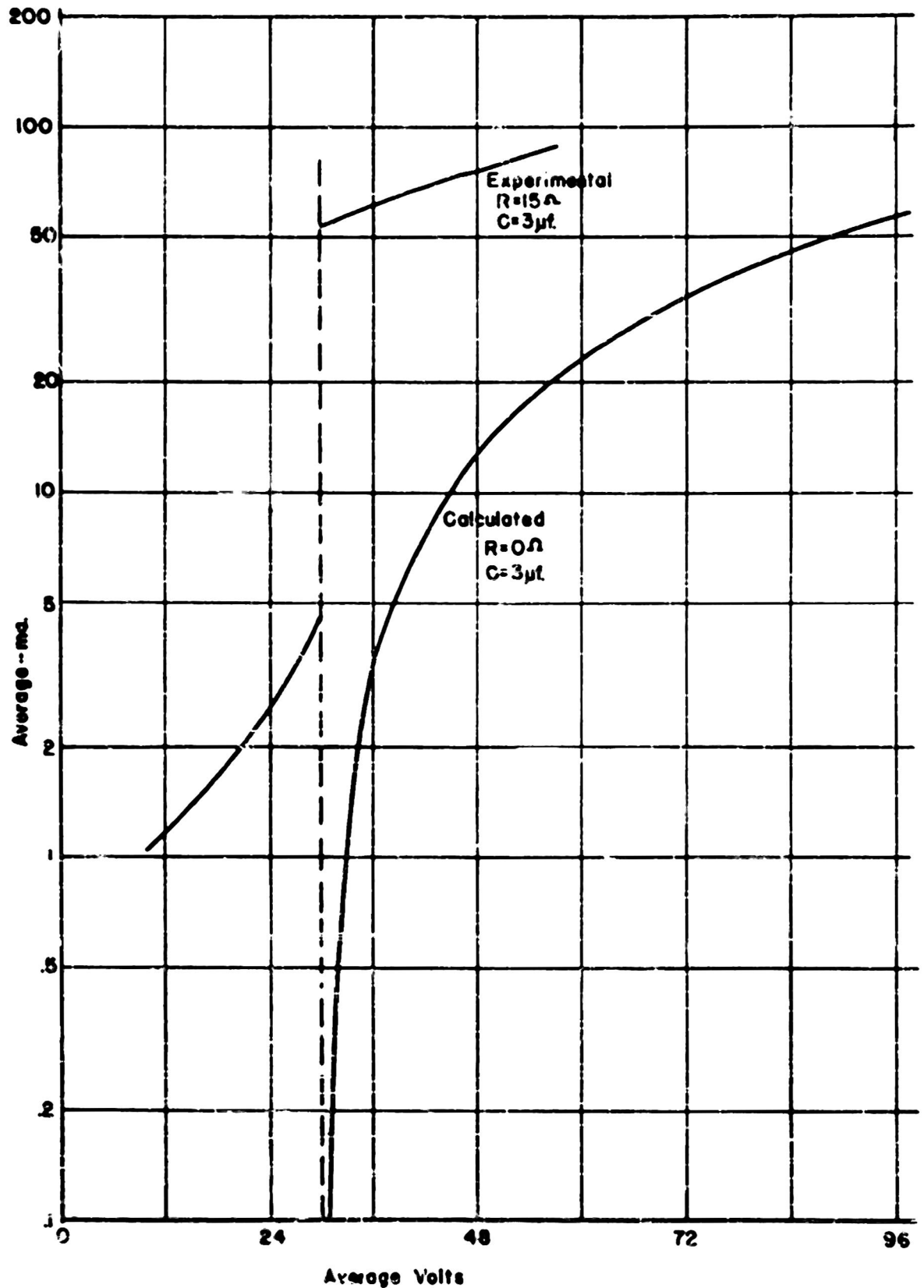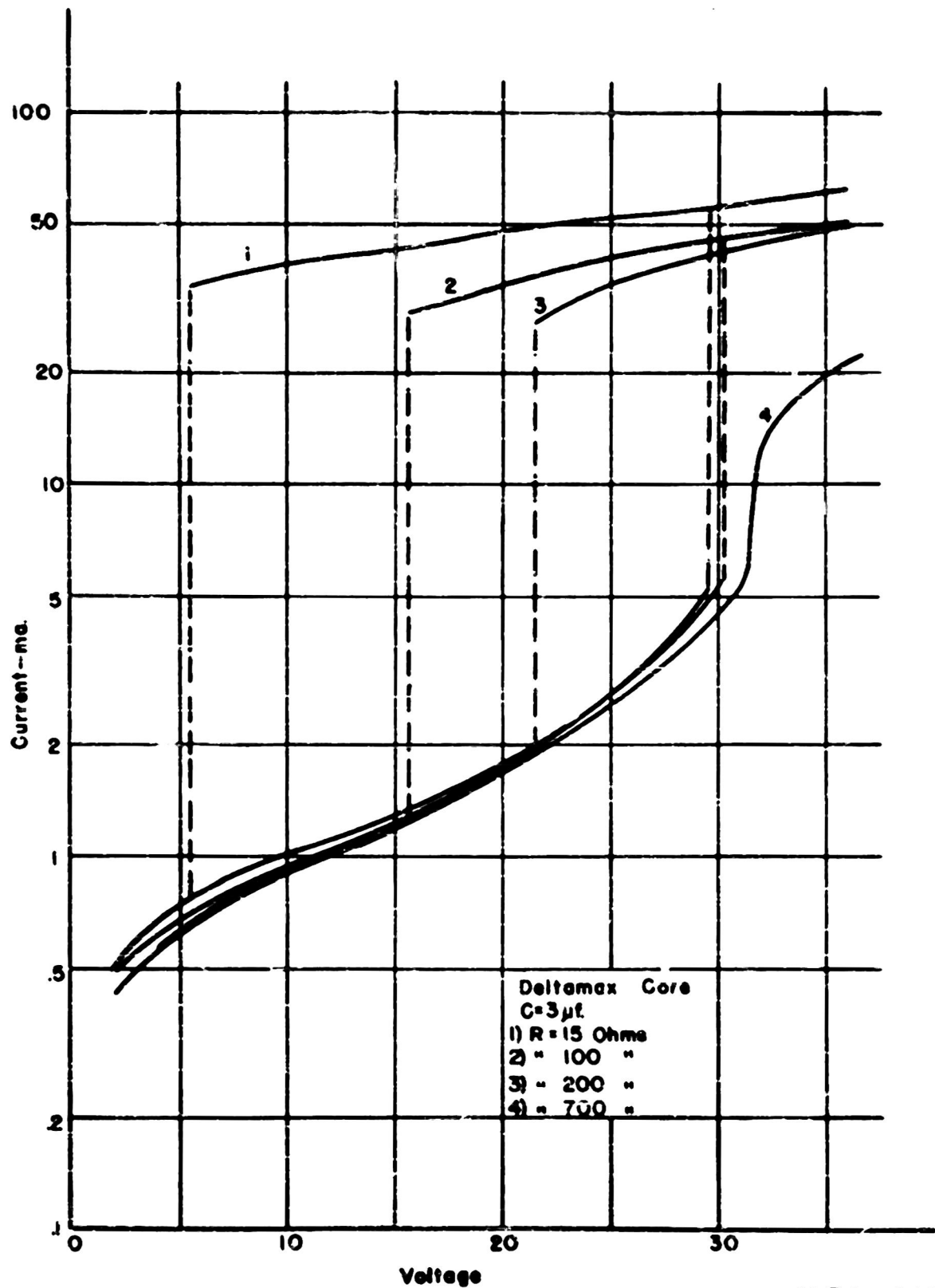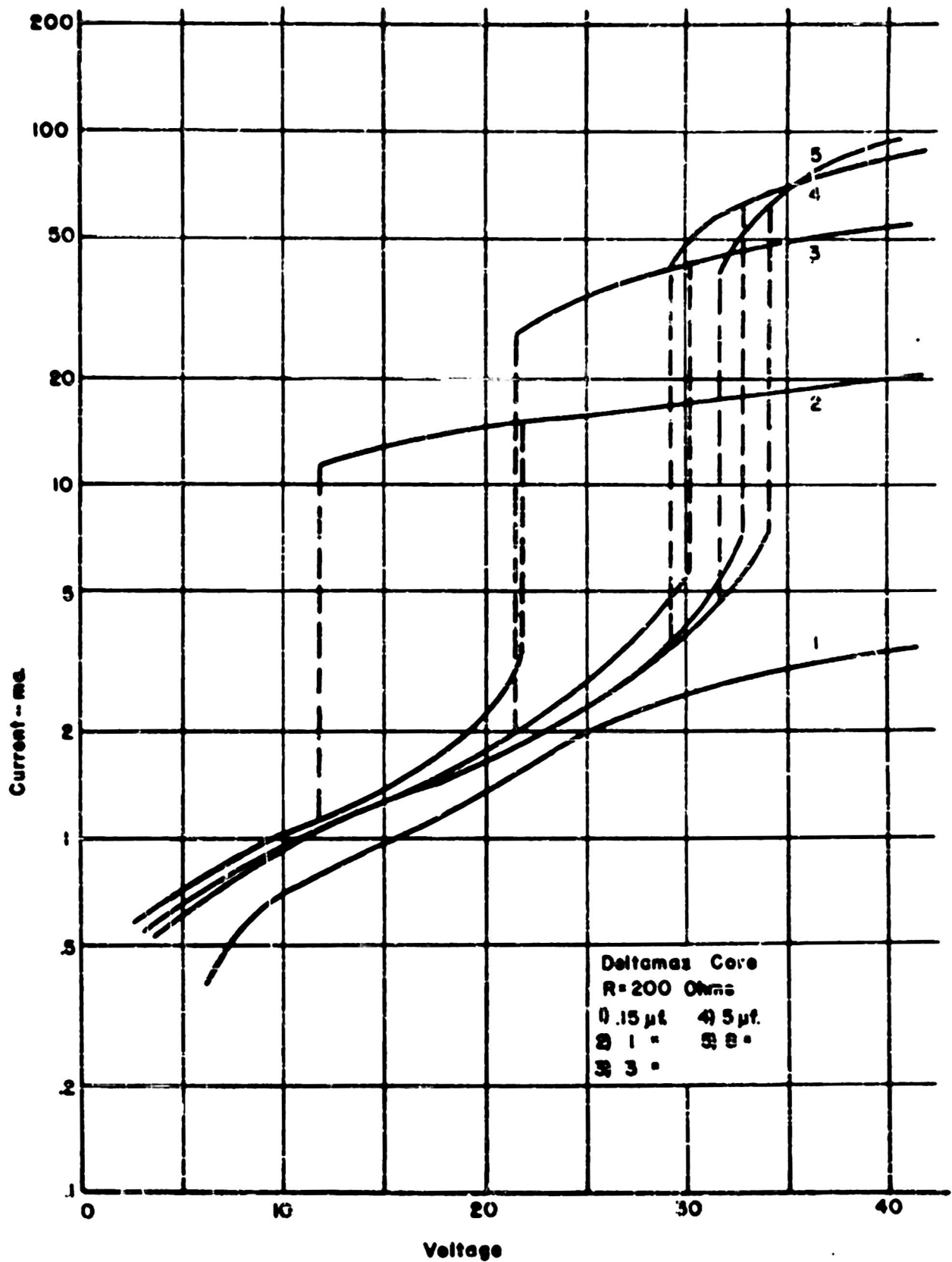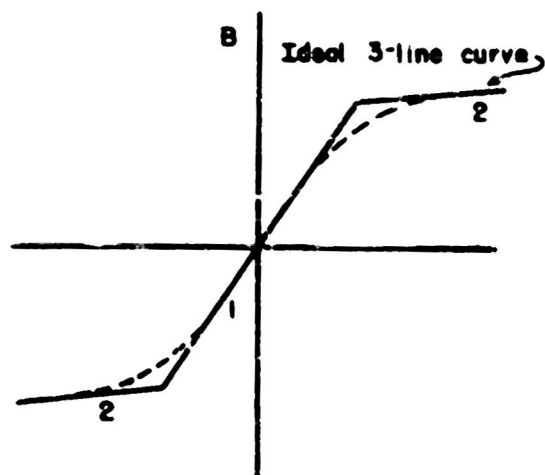
(a)
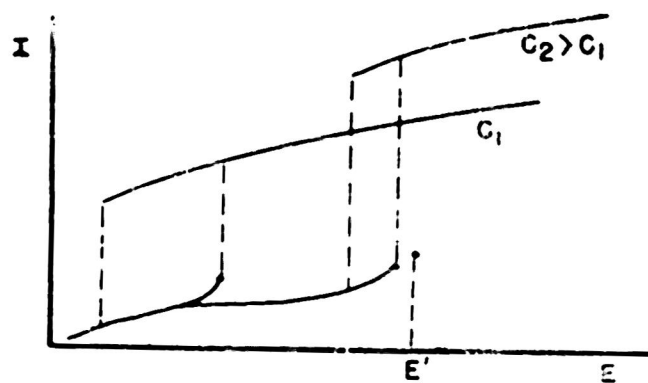
(b)
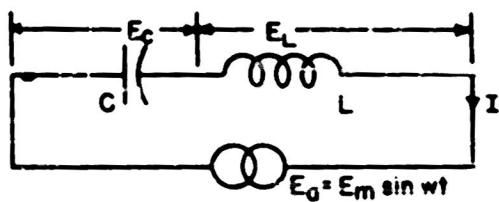
(c)
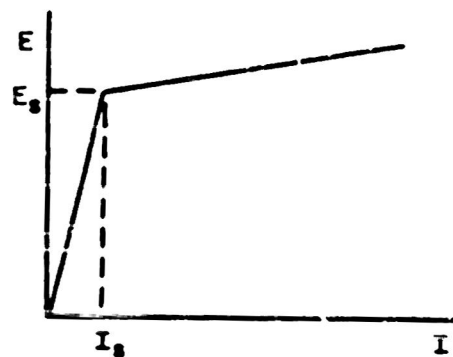
(d)
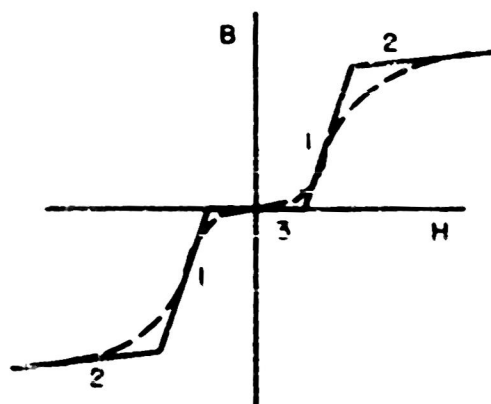
(e)

# LOW CURRENT CHARACTERISTIC OF THE SERIES CIRCUIT

Deltamax

R=200 Ohms

C=3 µf

Experimental ——

Calculated - - - -
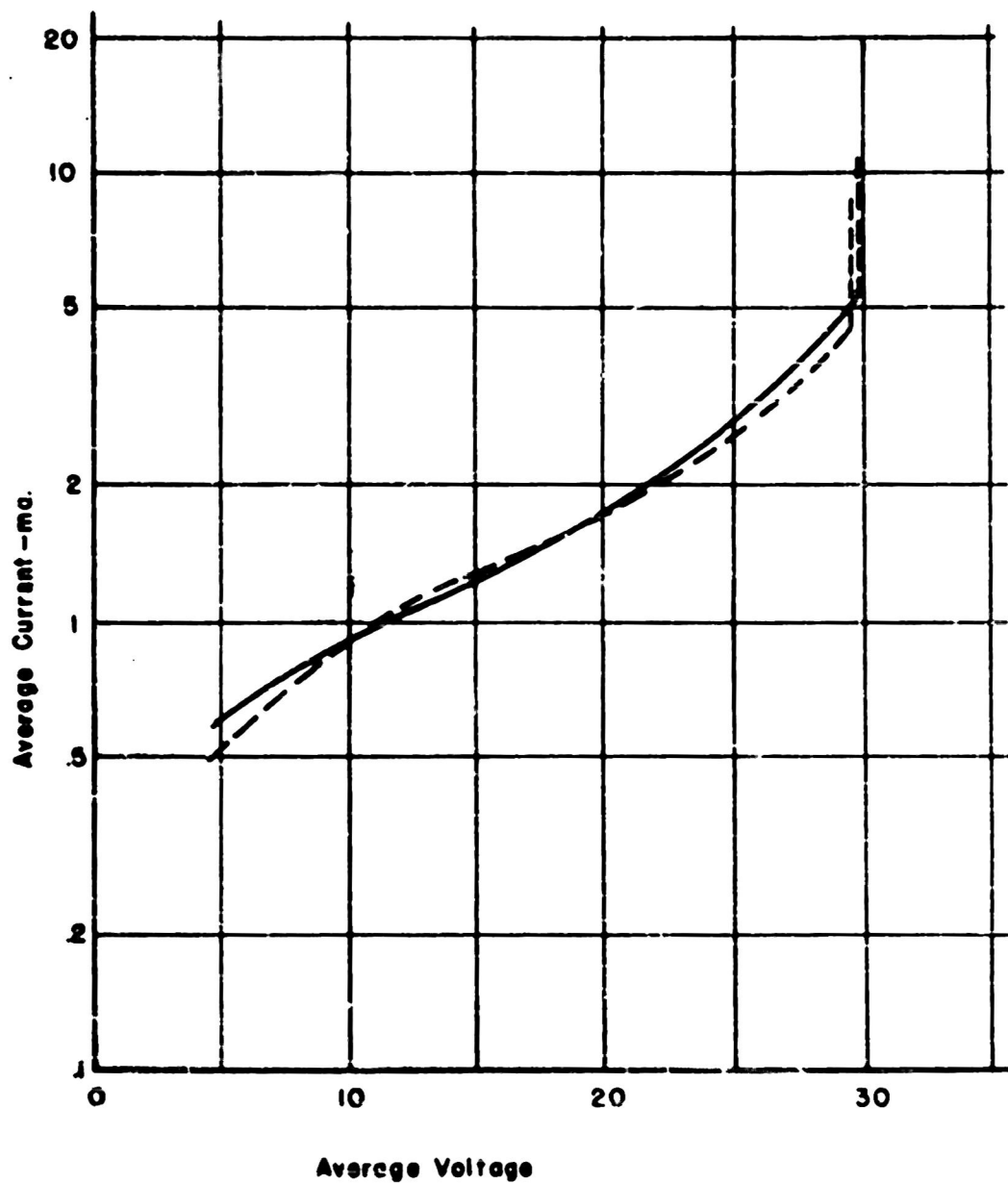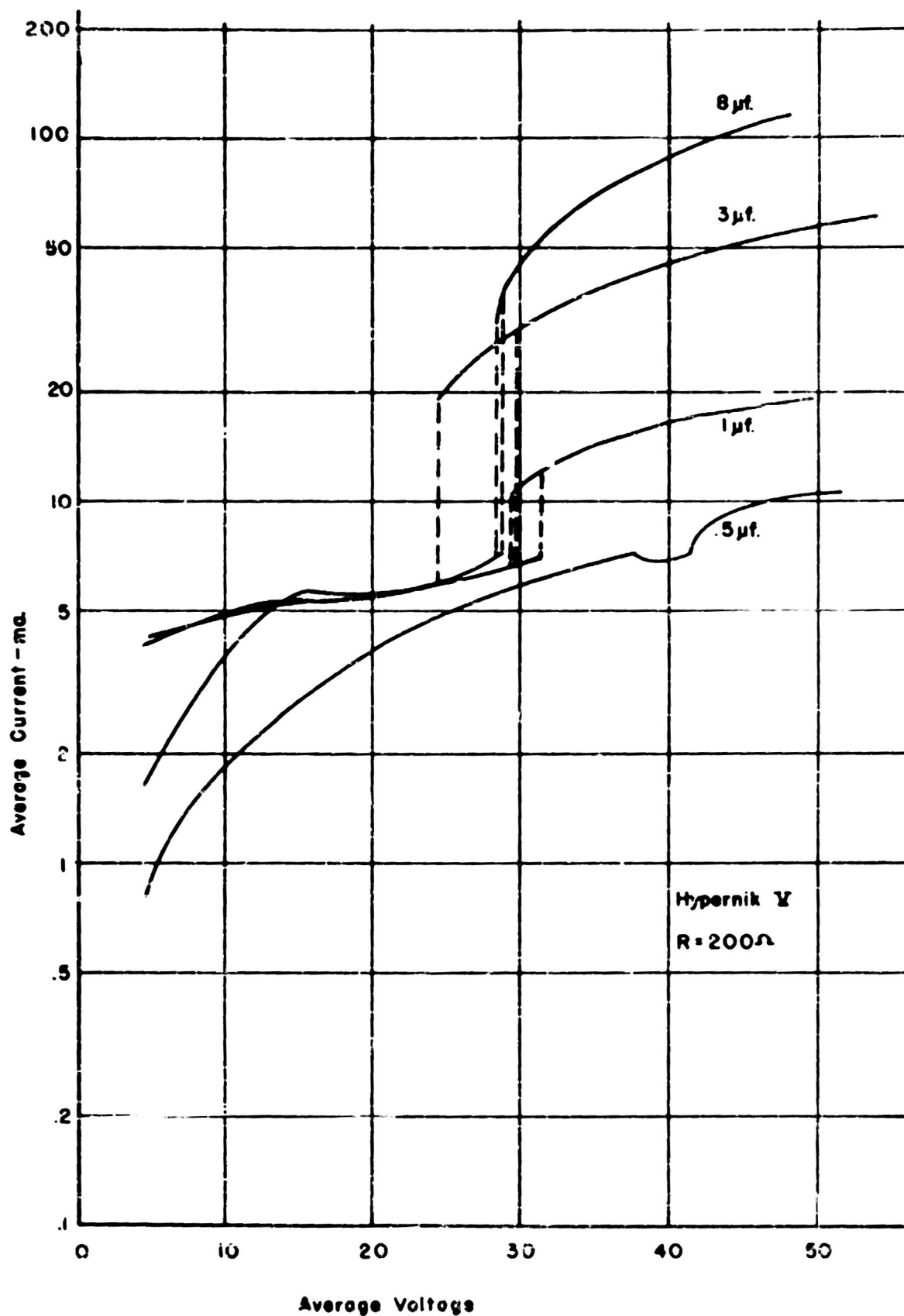
VOLT-AMPERE CHARACTERISTIC OF THE SERIES CIRCUIT
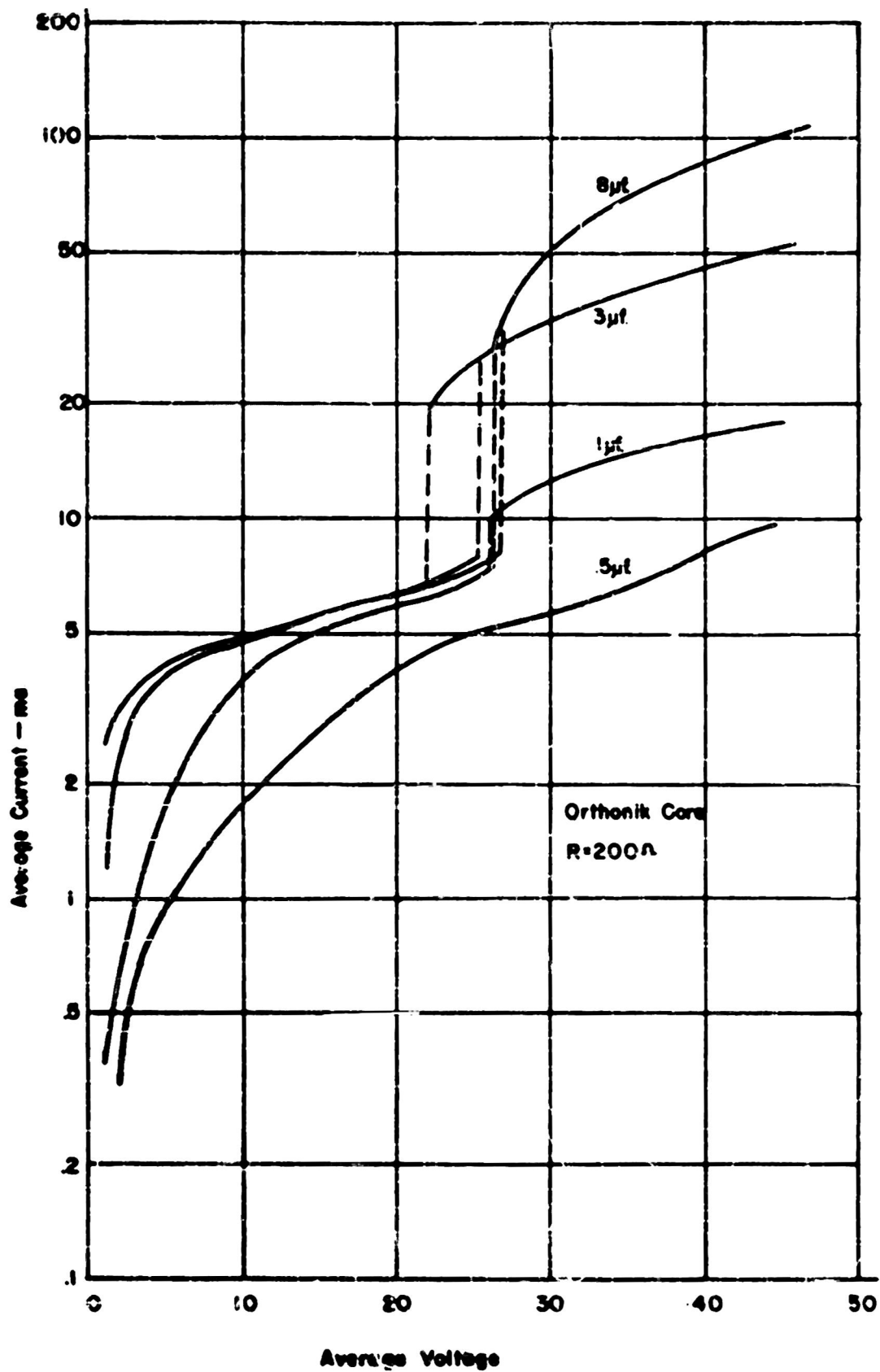
Deltamax Core

$C = 3 \mu f.$

$R = 15 \Omega$



(a)



(b)



(c)

M.R.I.-12503
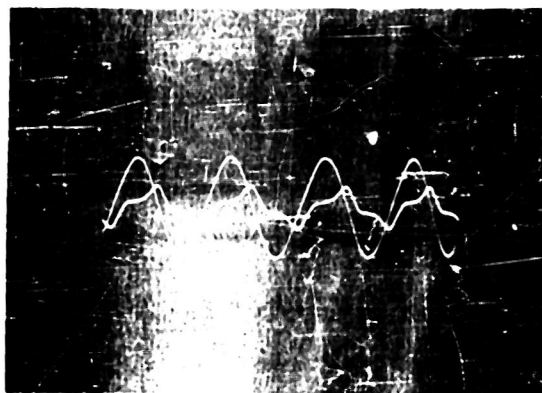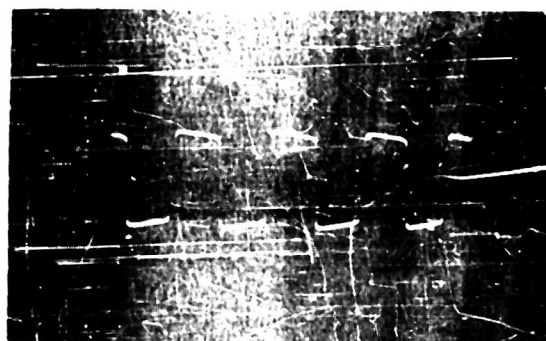
Deltamax Core
E = 55 V.



(a)



(b)

E = 110 V.



(c)



(d)

9-52

M.R.L- 2504
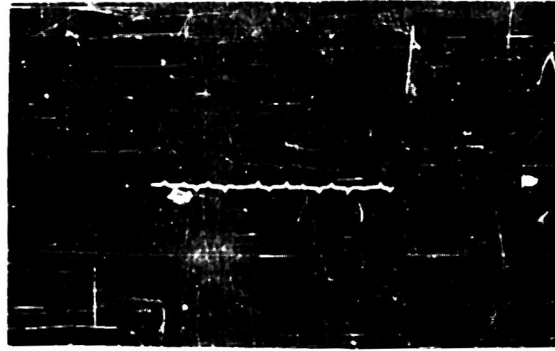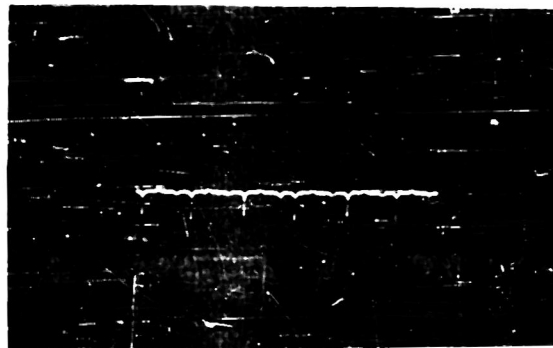
# ADDITIONAL MODES OF OPERATION COMMON TO THE SERIES
# FERRORESONANT CIRCUIT
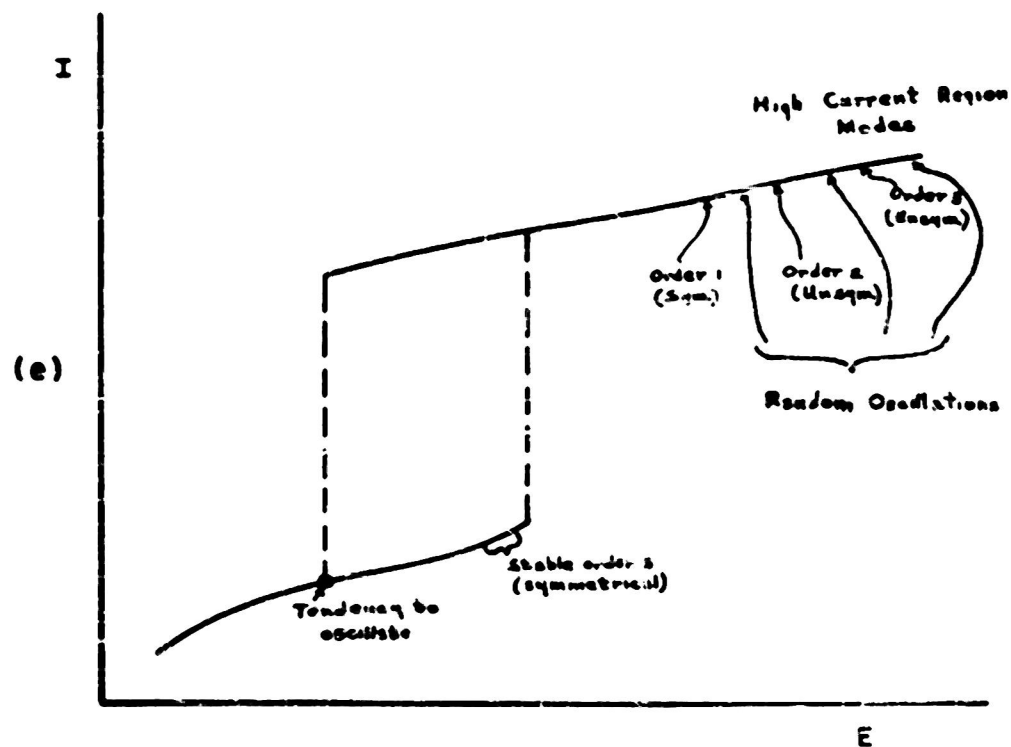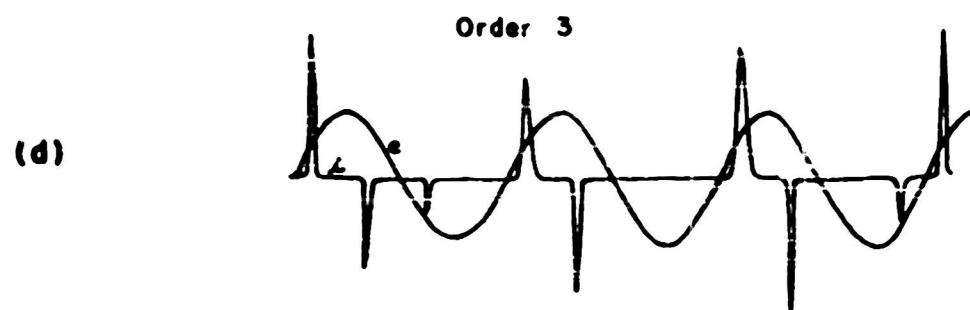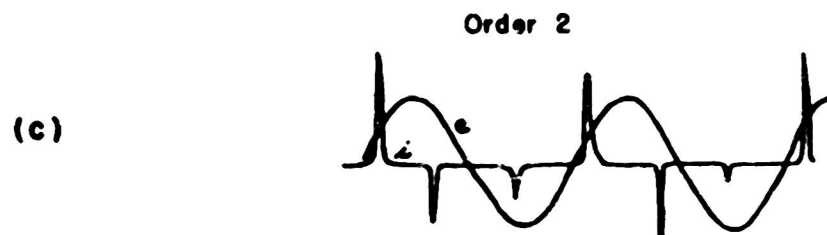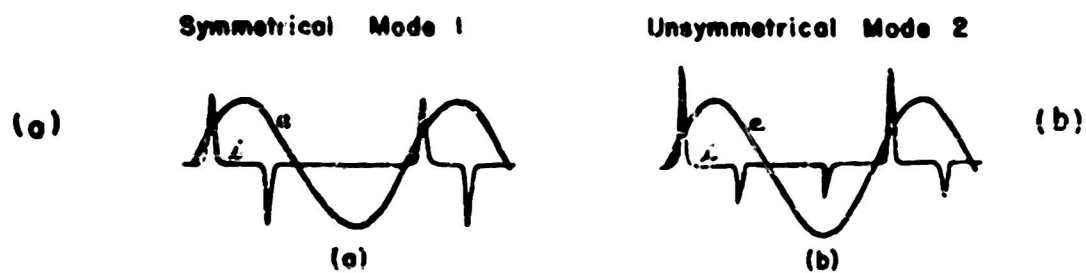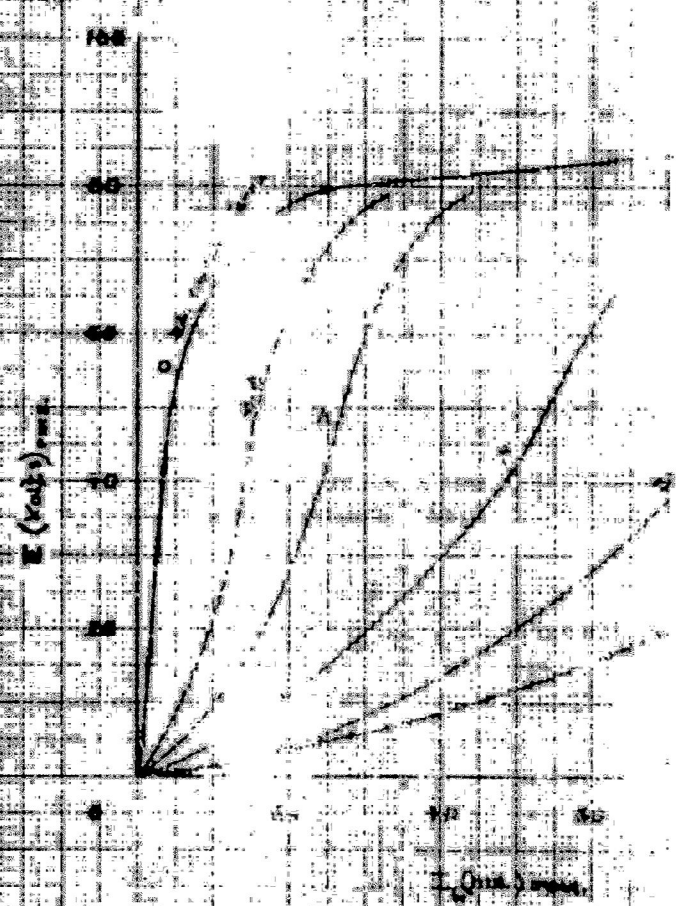
M.R.I.-12505

DELTA MAX REACTOR VOLT AMPERE CHARACTERISTICS WITH D.C. BIAS

9.52

NRL 19505

CONTROL CHARACTERISTICA ... PITAMAK REACTOR

$N_1 = M_0 = 700$ Turns

(a)

(b)
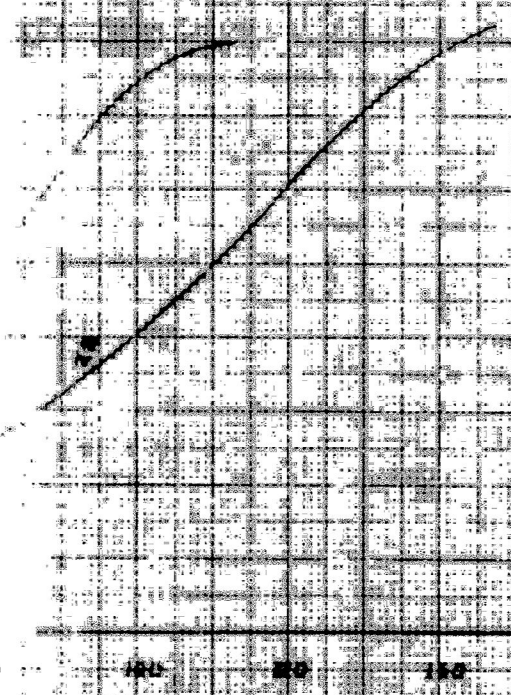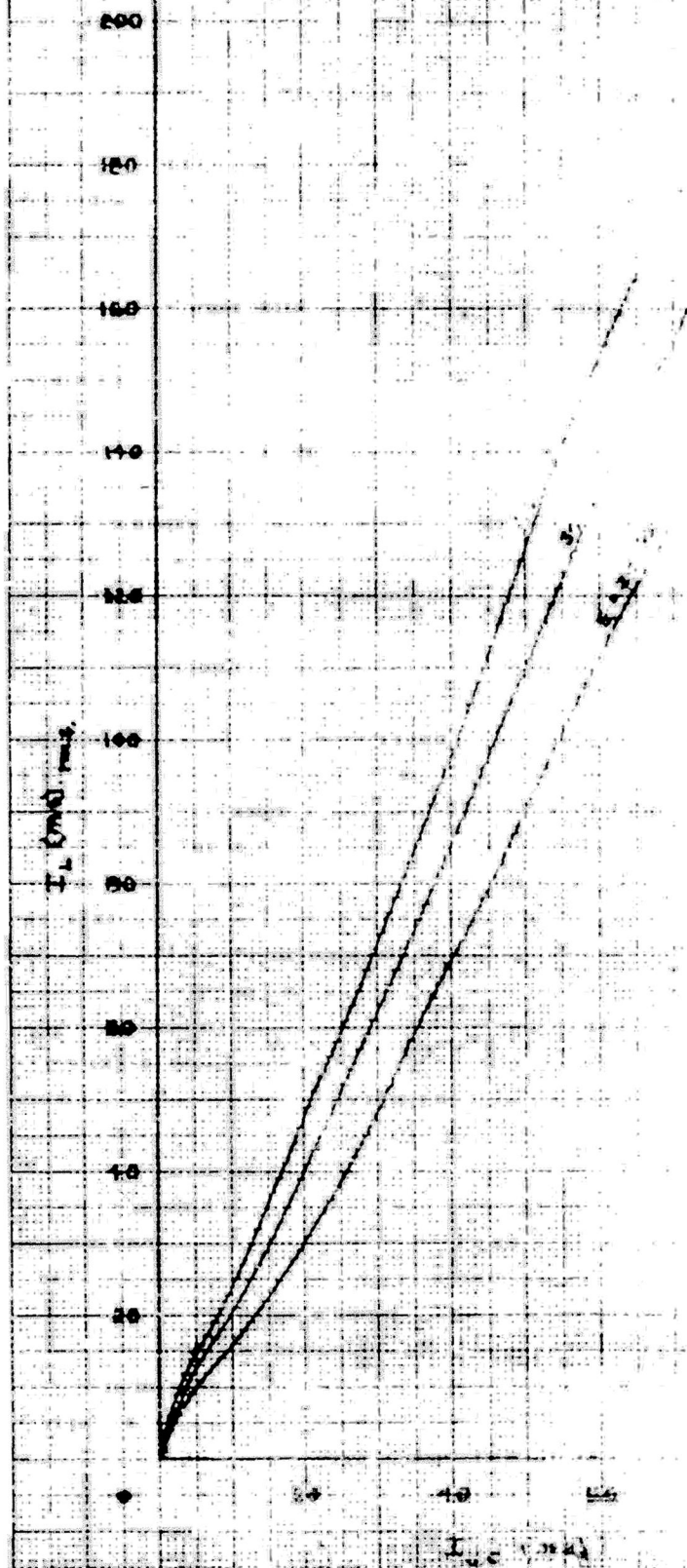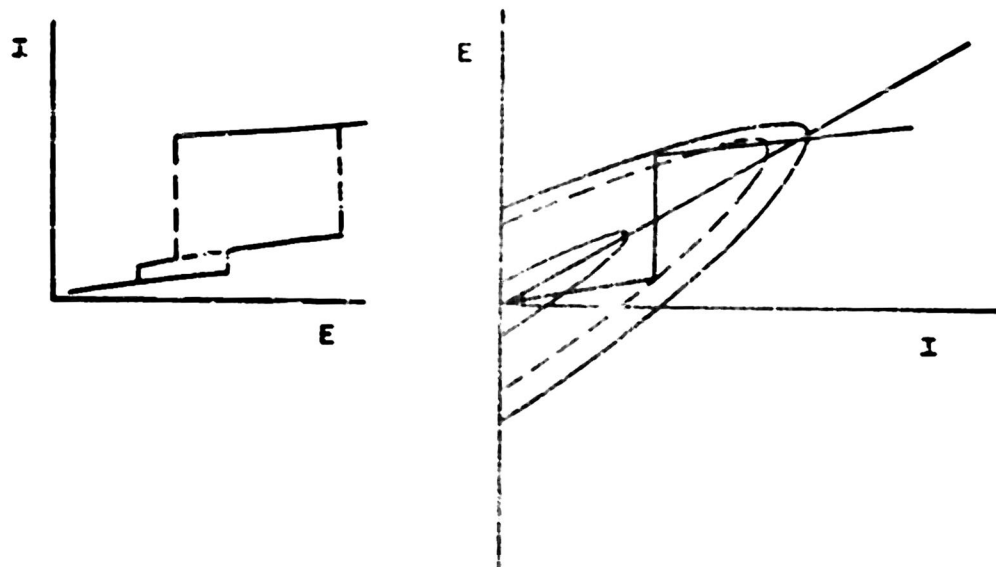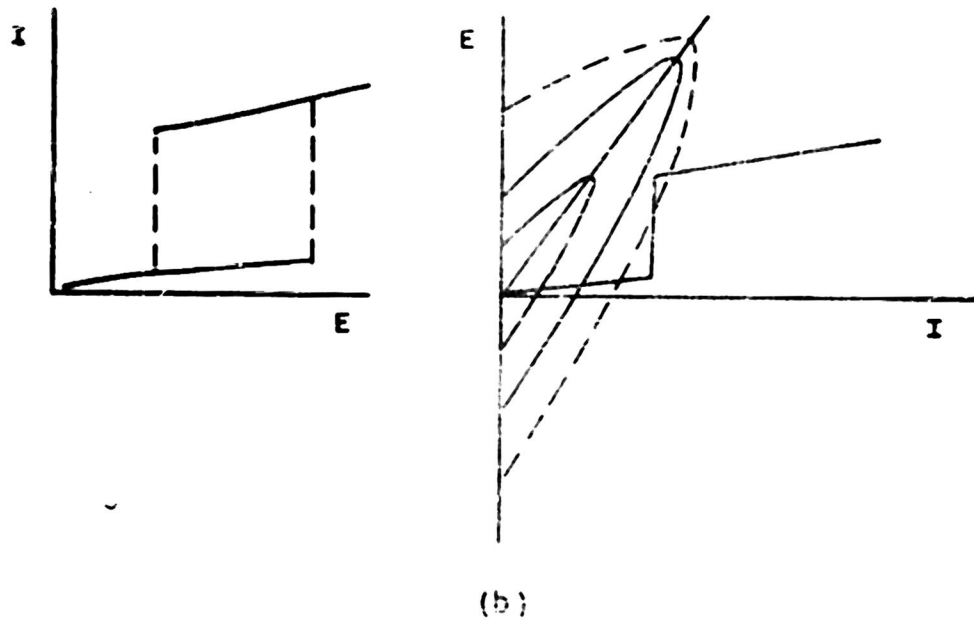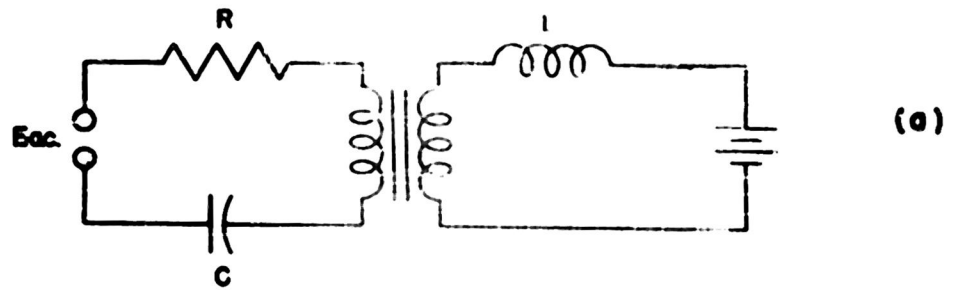
CONTROL CHARACTERISTIC OF THE SERIES CIRCUIT
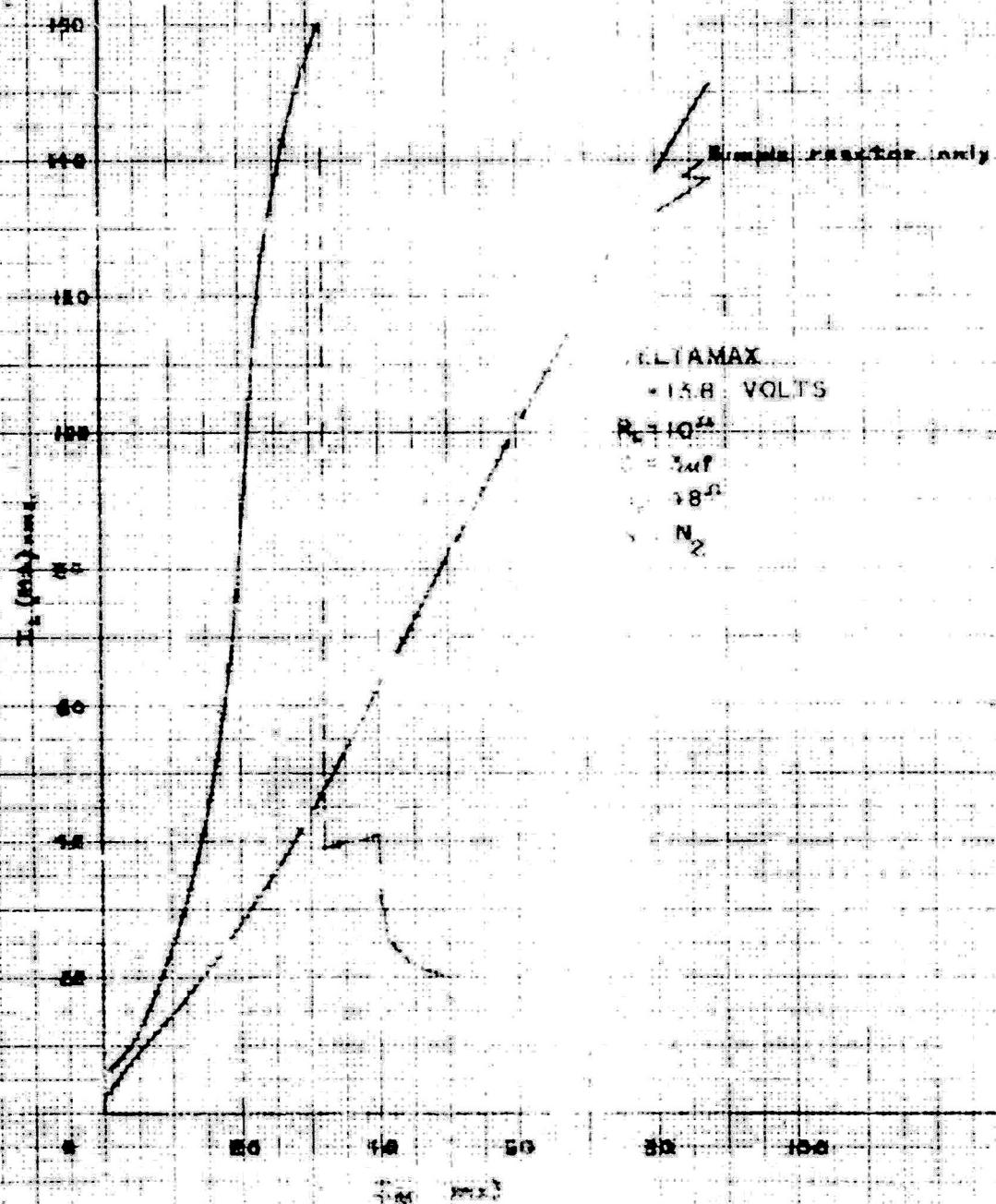
# TRANSIENT RESPONSE OF THE SERIES FERRORESONANT AMPLIFIER CIRCUIT
## AND THE SIMPLE REACTOR AMPLIFIER

(a)
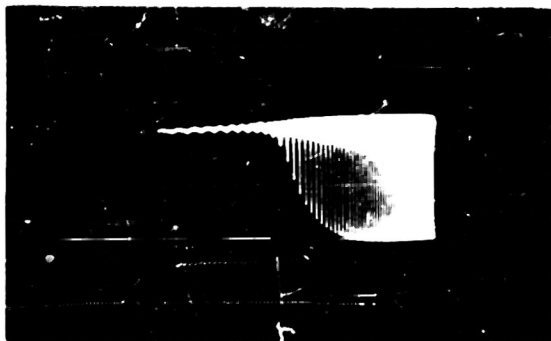


Buildup = .23 secs.
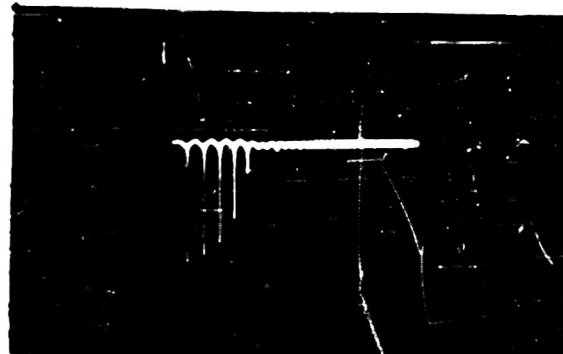


Decay =.083 secs.

Deltamax Cores

$E = 13.8$ v.

$C = 3$ µf.

$R_L = 13 \Omega$

$R_C = 48 \Omega$

$L_C = 7$ hy.

$N_C = N_L = 700$ turns

Signal = 0—31 ma.

(b)
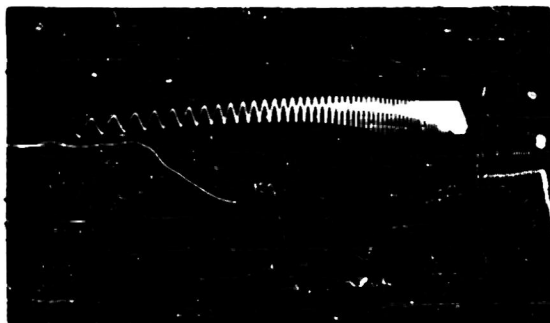


Buildup = .72 secs.
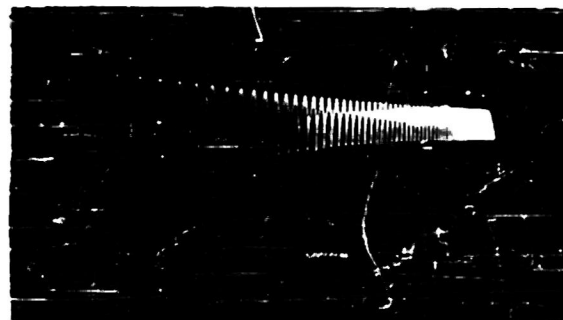


Decay = .2 secs.

$C = \infty$

Signal = 0—31 ma.

CONTROL CHARACTERISTIC OF THE SERIES CIRCUIT
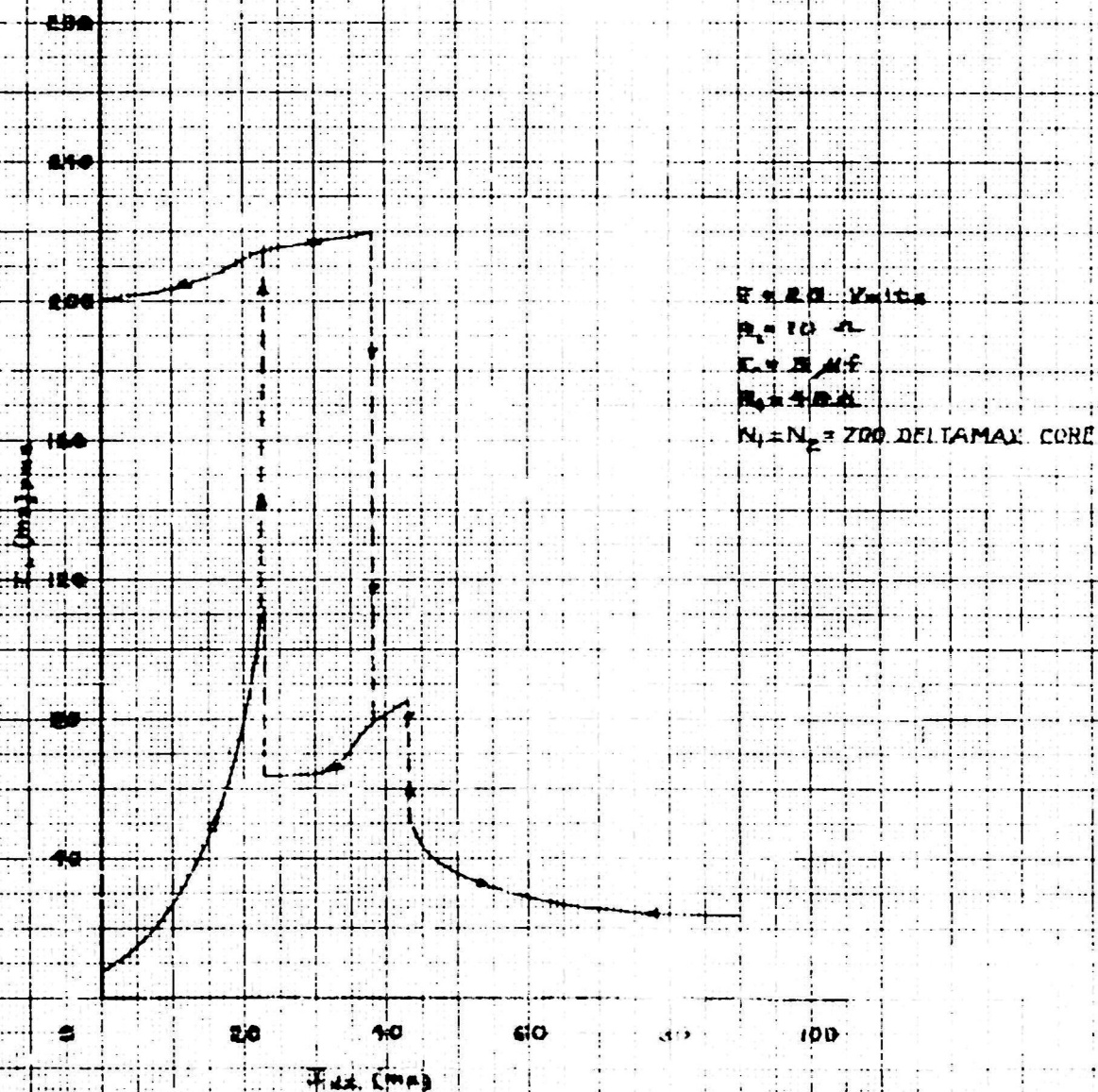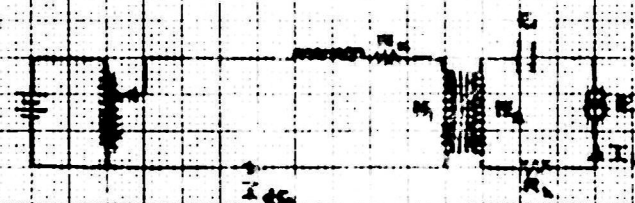
$E = 2.0$ Volts
$R_s = 10$ A.
$C = 5$ Mf.
$R_L = 50$ A.
$N_1 = N_2 = 200$ DELTAMAX CORE

M.R.I. 12511
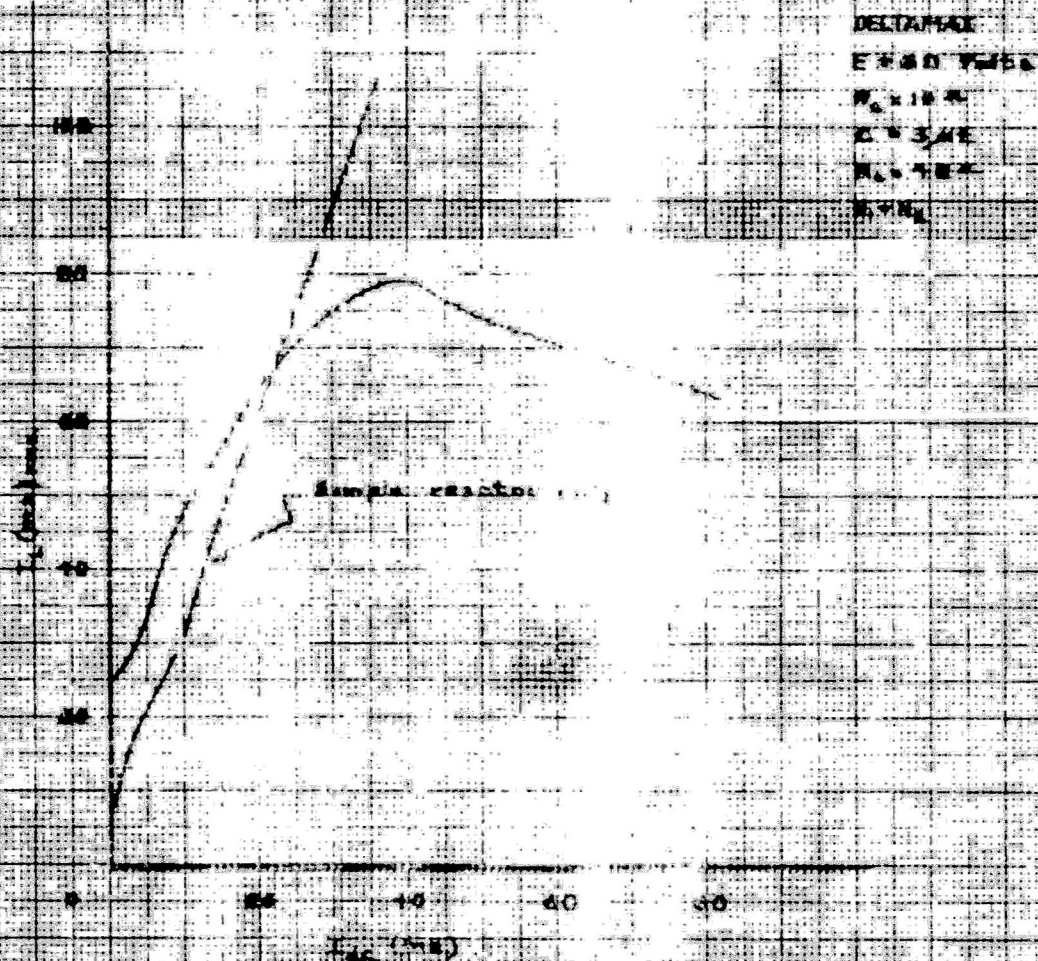
CONTROL CHARACTERISTIC OF THE SERIES CIRCUIT
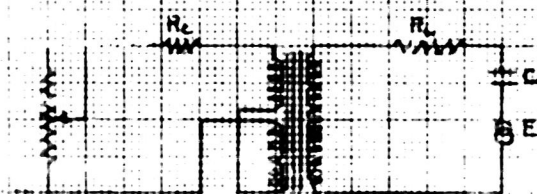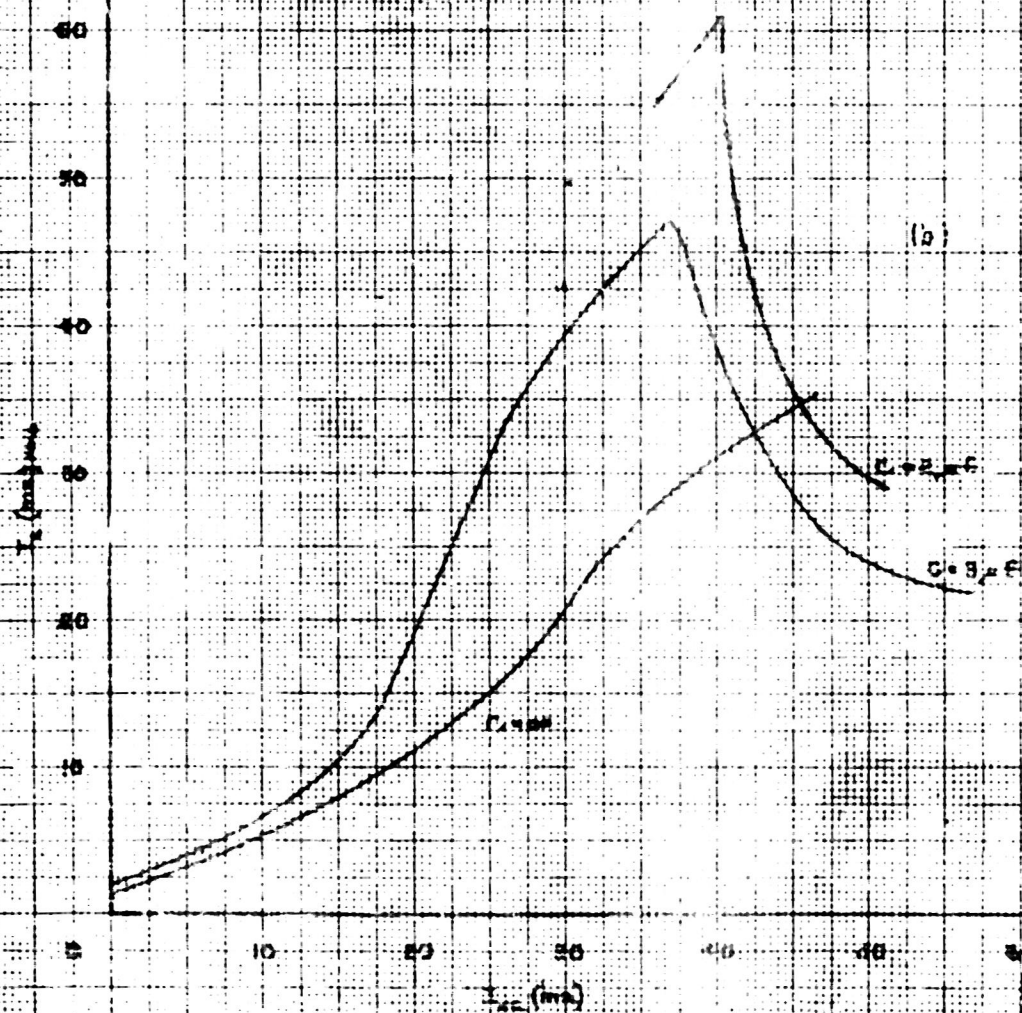
# TRANSIENT RESPONSES OF THE DOUBLE-CORE SIMPLE REACTOR AND SERIES FERRORESONANT CIRCUITS

(a)



$C = \infty$
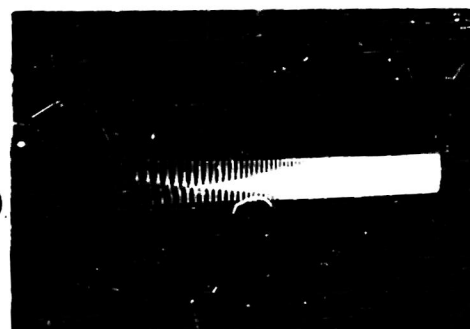
Signal = 38—48 ma. (d.c.)

Deltamax Cores
$E = 16v.$
$R_c = 260\,\Omega$
$R_c = 16\,\Omega$
$N_1 = N_2$ turns

Buildup = .12 secs.

Decay = .12 secs.



Signal = 38—48 ma. (d.c.)

$C = 3\mu f.$

(b)

Buildup
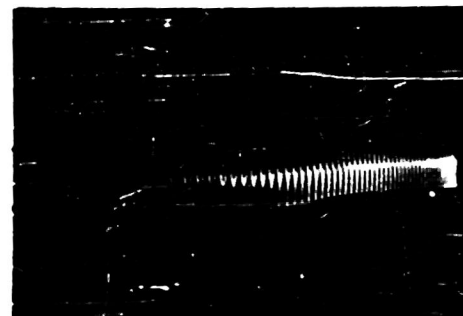
Decay
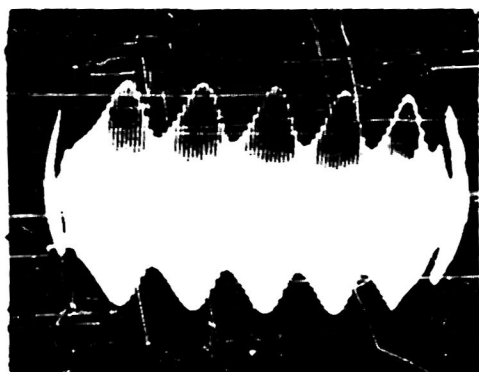


Carrier = 60 $\sim$
Subharmonic = 3.5 $\sim$

(c)

Carrier = 60 $\sim$
Mark = .23 secs.
Space = 48 —

(d)

M.R.I.-12514

AMPLIFICATION BY MEANS OF FERRORESONANCE
( Constrained )

Deltamax

E = 120 Volts
$R_L$ = 800 Ohms
60 cps.

1) C = ∞ µf.
2) C = 3

RMS. LOAD CURRENT - MA.

D-C CONTROL CURRENT - M.A.

M.R.I.- 12515
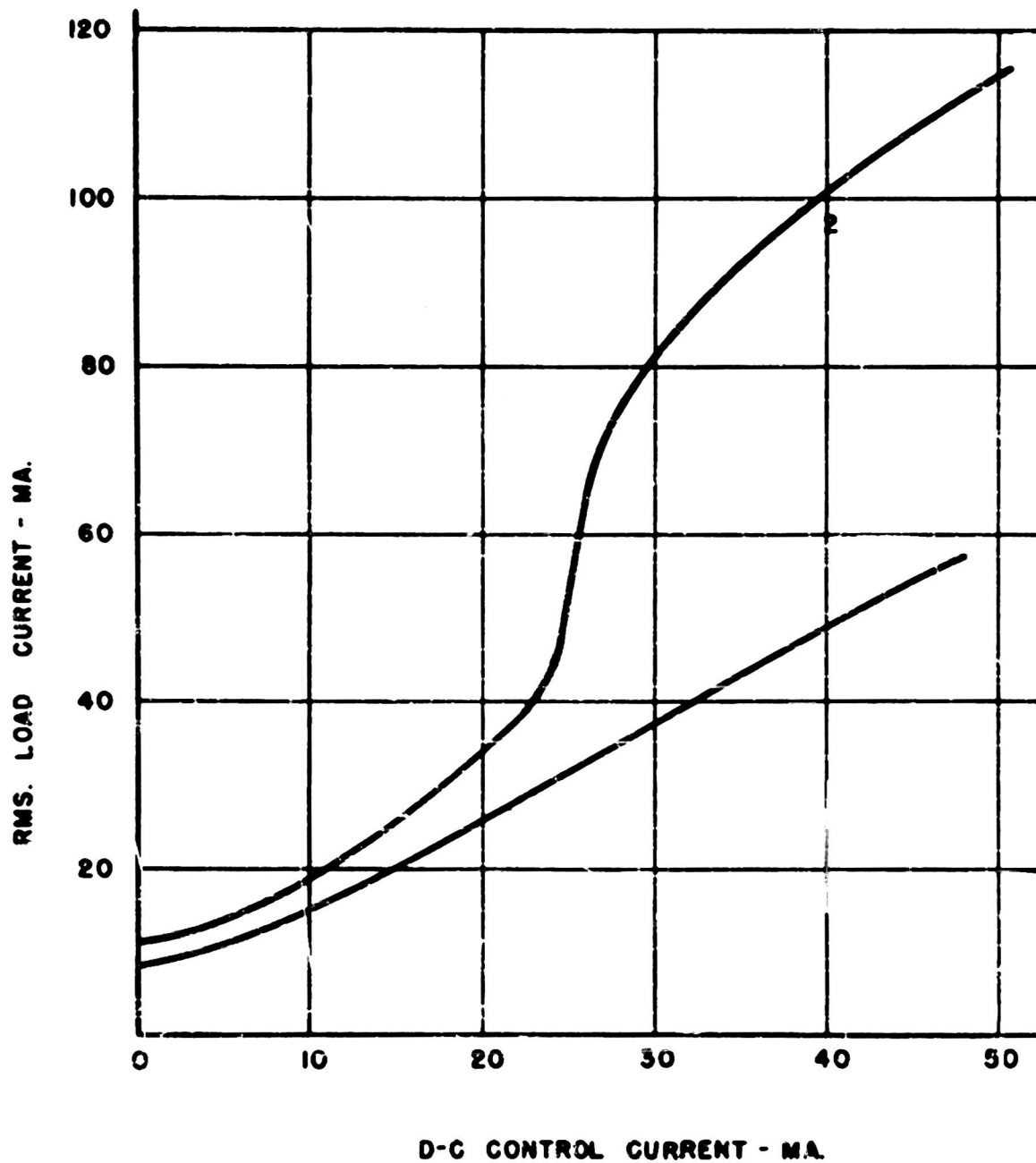
# TRANSIENT RESPONSES OF THE SIMPLE REACTOR AND THE SERIES FERRORESONANT CIRCUITS

## (Constrained)
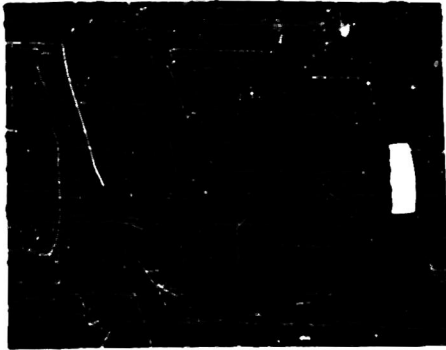


Buildup = .14 secs.

Deltamax Cores

Signal = 19—32 ma. (dc.)

$R_L$ = 800 $\Omega$

(a)
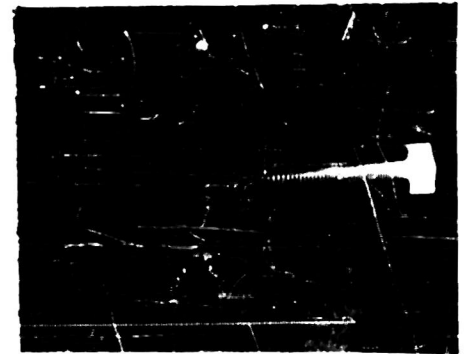


Decoy = .4 secs.
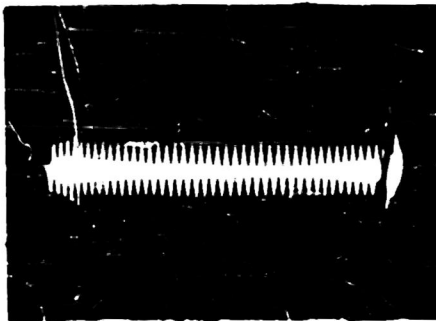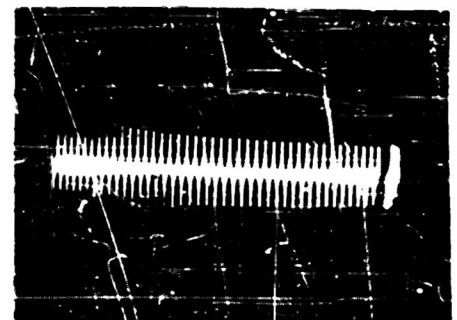


Buildup = .12 secs.

Signal = 19—32 ma.

C = 3 μf.

$R_L$ = 800 $\Omega$

(b)



Decoy = .4 secs.



Buildup = .22 secs.
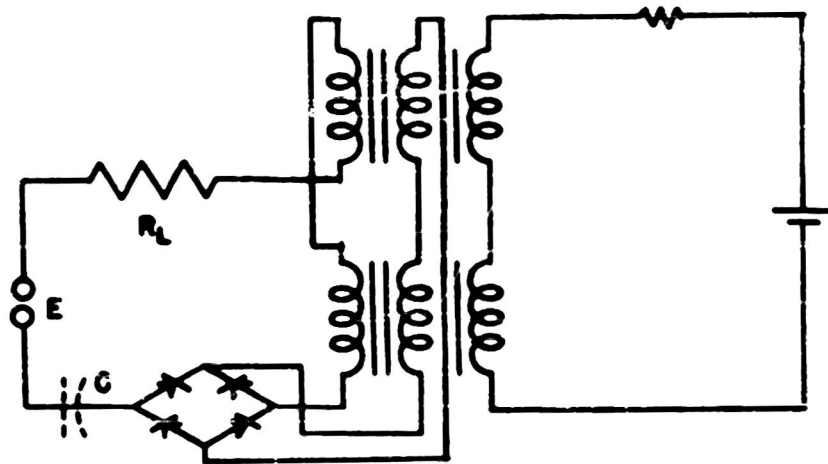
Signal = 19—32 ma.

C = 3 μf.

$R_L$ = 930 $\Omega$
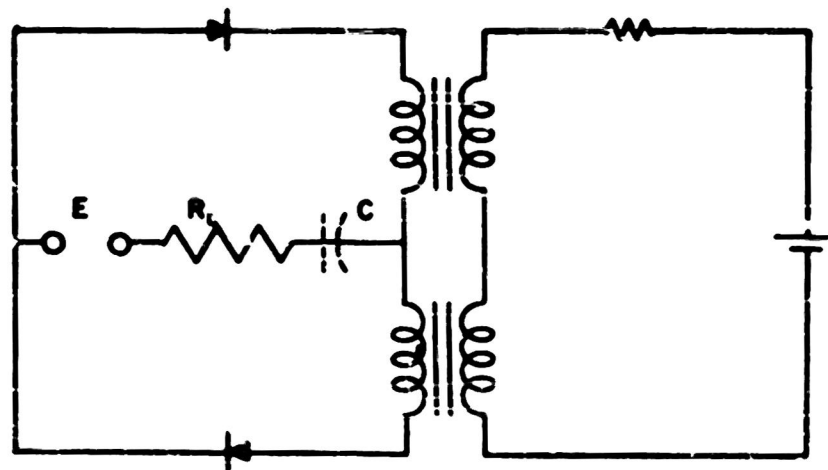
(c)



Decoy = .14 secs.

(A)
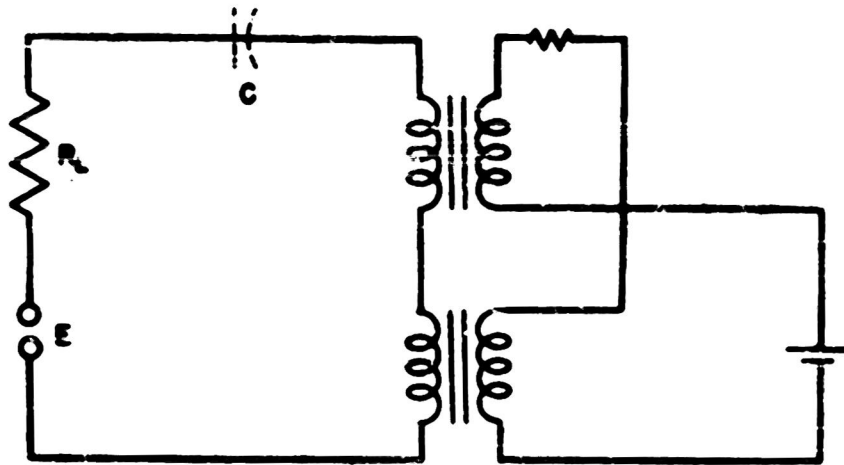
(B)

(C)

A) SIMPLE SATURABLE REACTOR CIRCUIT
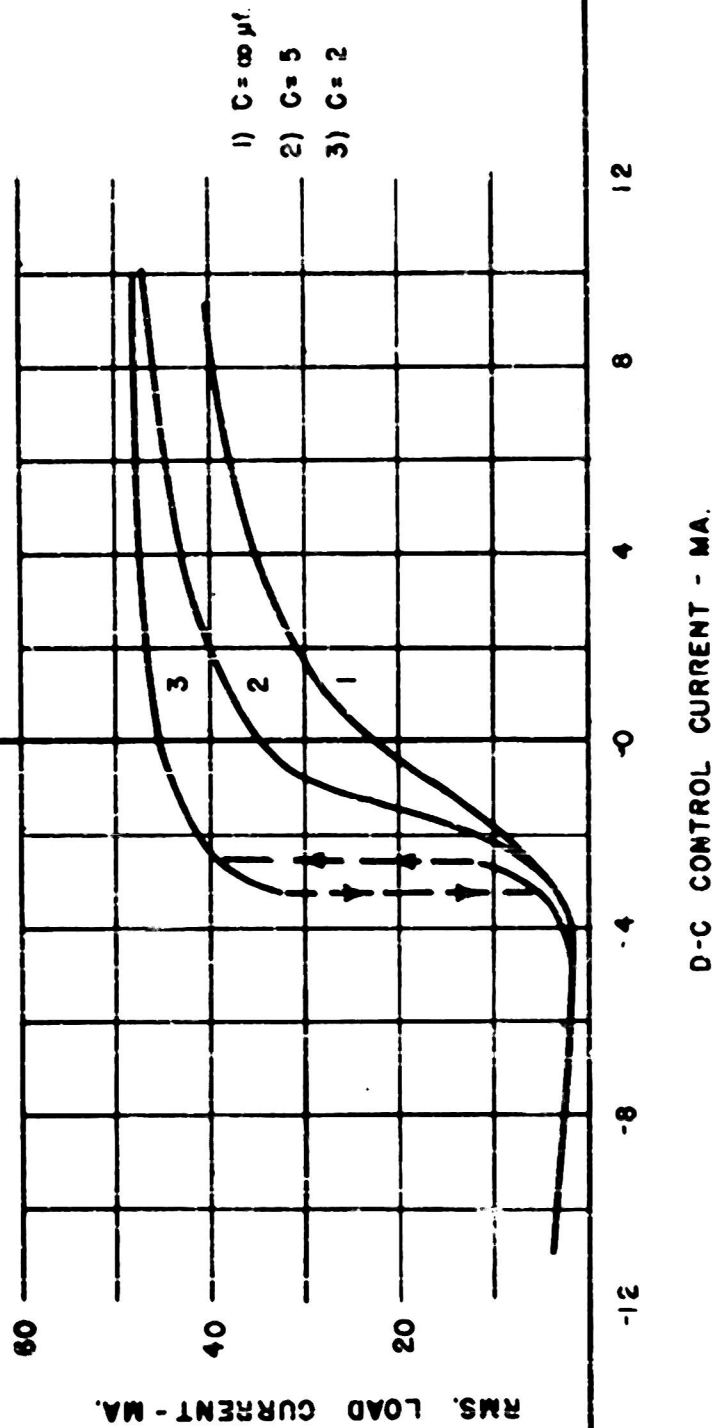B) EXTERNAL FEEDBACK AMPLIFIER
C) DOUBLER CIRCUIT

M.R.I.-12517

EXTERNAL FEEDBACK AMPLIFIER EMPLOYING FERRORESONANCE
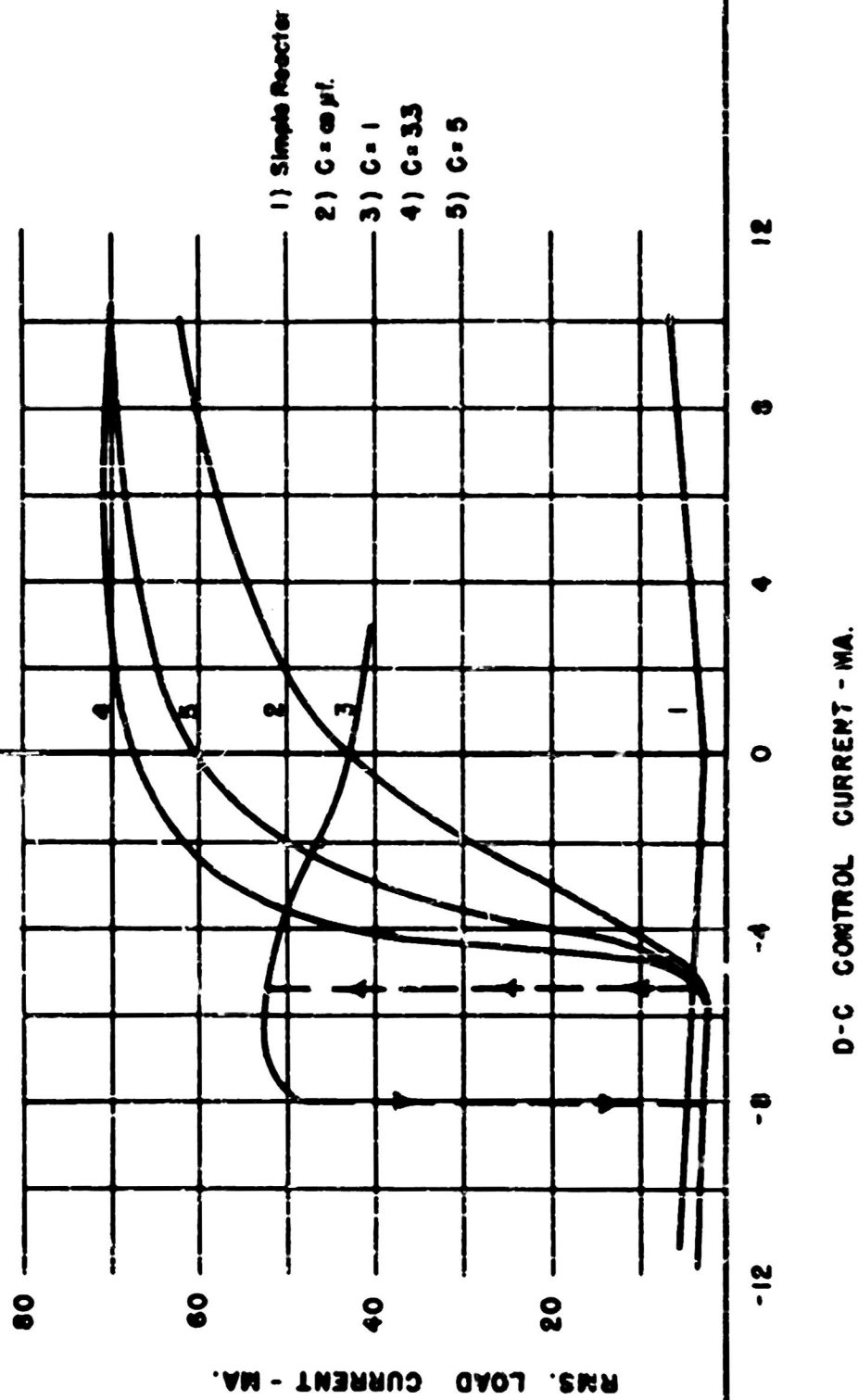(UNCONSTRAINED)

HYMU 80   TYPE DU-1 CORES

E = 10V.
R_L = 140 Ohms
400 cps.

1) C = ∞ μf.
2) C = 5
3) C = 2

D-C CONTROL CURRENT - MA.

RMS. LOAD CURRENT - MA.

9-52

M.R.L-1251B

# SATURABLE REACTOR CIRCUIT EMPLOYING FERRORESONANCE AND EXTERNAL FEEDBACK
## (CONSTRAINED TRANSFER CURVES)

HYMU 80 TYPE DU-1 CORES

1) Simple Reactor
2) C = ∞ μf.
3) C = 1
4) C = 3.3
5) C = 5

E = 10 V.
R₁ = 65 Ohms
400 cps.

D-C CONTROL CURRENT - MA.

RMS. LOAD CURRENT - MA.

EFFECT OF LINE VOLTAGE VARIATIONS ON EXTERNAL FEEDBACK CIRCUIT (UNCONSTRAINED)

R_L = 140 Ohms
400 cps

HYMU 80 TYPE DU-1 CORES

RMS. LOAD CURRENT - MA.

D-C CONTROL CURRENT - MA.

12 V.
10 V.
8 V.
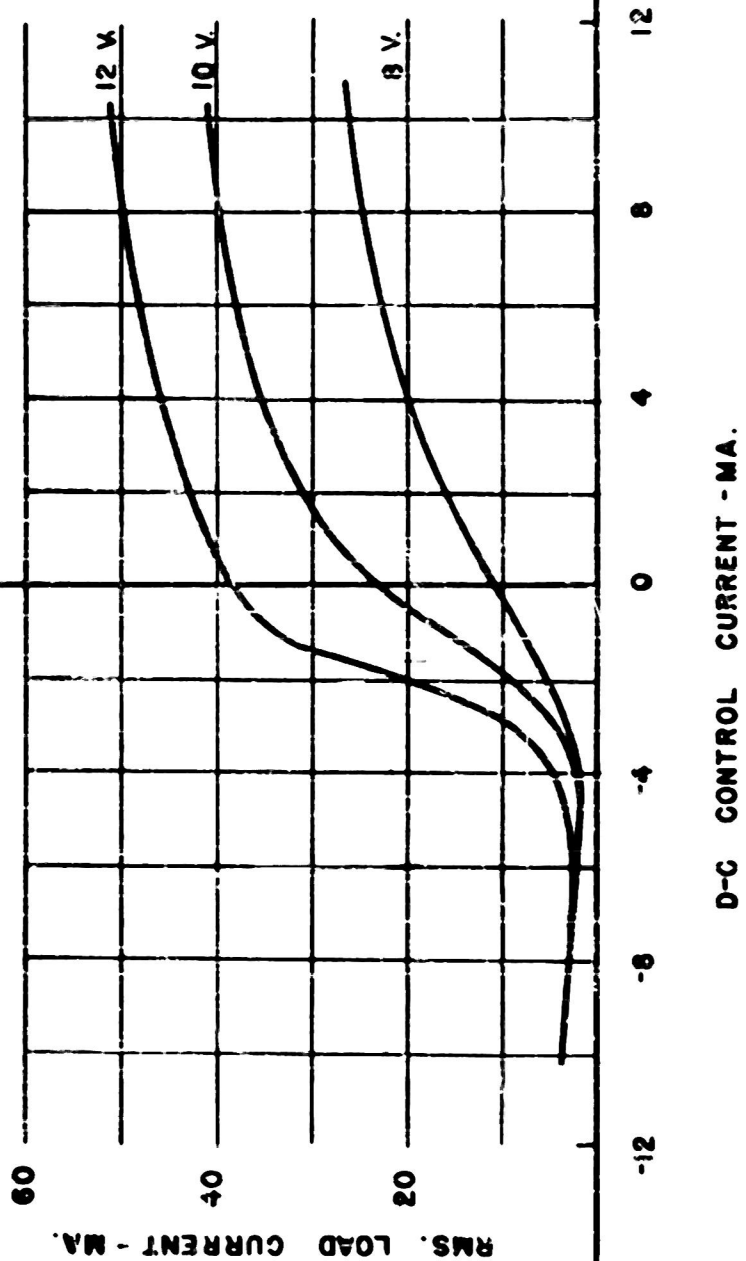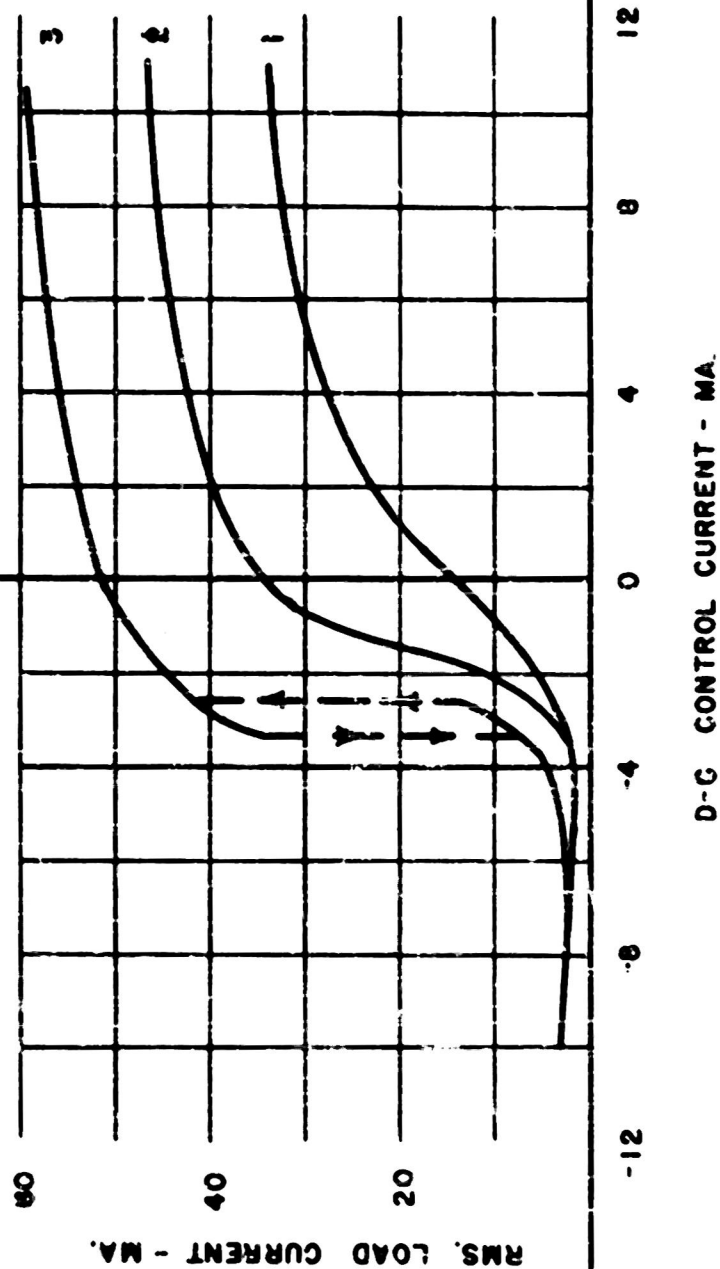
EFFECT OF LINE VOLTAGE VARIATIONS ON EXTERNAL FEEDBACK AMPLIFIER EMPLOYING FERRORESONANCE

HYMU 80 TYPE DU-1 CORES

1) E = 8 Volts
2) E = 10
3) E = 12

C = 5 μf.
R_L = 140 Ohms
400 cps.

RMS. LOAD CURRENT - MA.
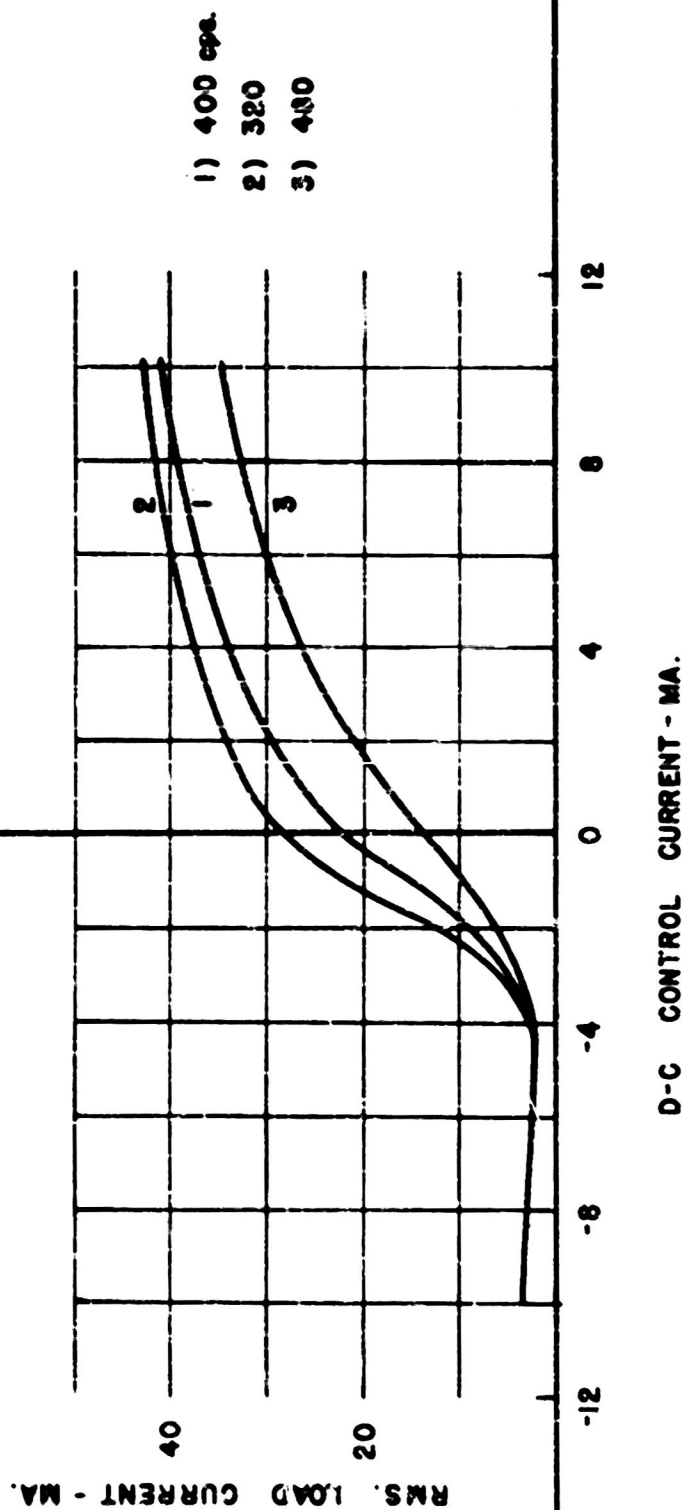
D-C CONTROL CURRENT - MA.

EFFECT OF FREQUENCY VARIATIONS ON EXTERNAL FEEDBACK CIRCUIT (UNCONSTRAINED)

HYMU 80   TYPE DU-I CORES

E = 10 V.

$R_L$ = 140 Ohms

1)  400 cps.
2)  320
3)  480

D-C CONTROL CURRENT - MA.

RMS. LOAD CURRENT - MA.

EFFECT OF FREQUENCY VARIATIONS ON EXTERNAL FEEDBACK AMPLIFIER EMPLOYING
FERRORESONANCE

HYMU 80 TYPE DU-1 CORES

E = 10 V.
C = 5 µf.

1) 400 cps.
2) 320
3) 480

# EFFECT OF FERRORESONANCE ON AN UNSTABLE EXTERNAL FEEDBACK AMPLIFIER
## (UNCONSTRAINED TRANSFER CURVES)

HYMU 80   TYPE DU-1 CORES

E = 10 V.

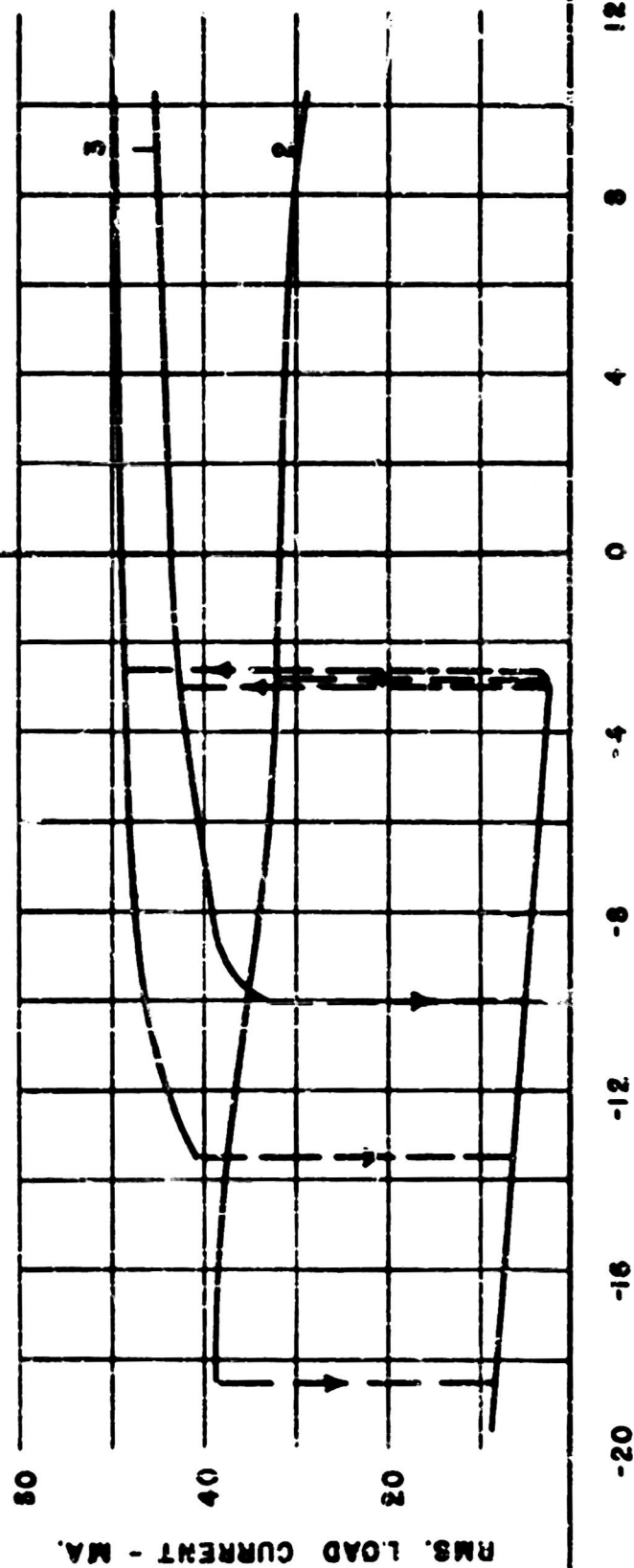$R_L$ = 140 Ohms

1) C = ∞ µf
2) C = 1
3) C = 8



RMS. LOAD CURRENT - MA.

D-C CONTROL CURRENT - MA.

TRANSFER CURVES OF DOUBLER CIRCUIT (UNCONSTRAINED)
ILLUSTRATING EFFECTS OF FERRORESOMANCE

1) C=∞ µf.
2) C=2
3) C=4

HYMU 80    TYPE DU-1 CORES

E = 8 V.
R_L = 100 Ohms
400 cps.

RMS. LOAD CURRENT - MA.

D-C CONTROL CURRENT - MA.

TRANSFER CURVES OF DOUBLER CIRCUIT (UNCONSTRAINED)
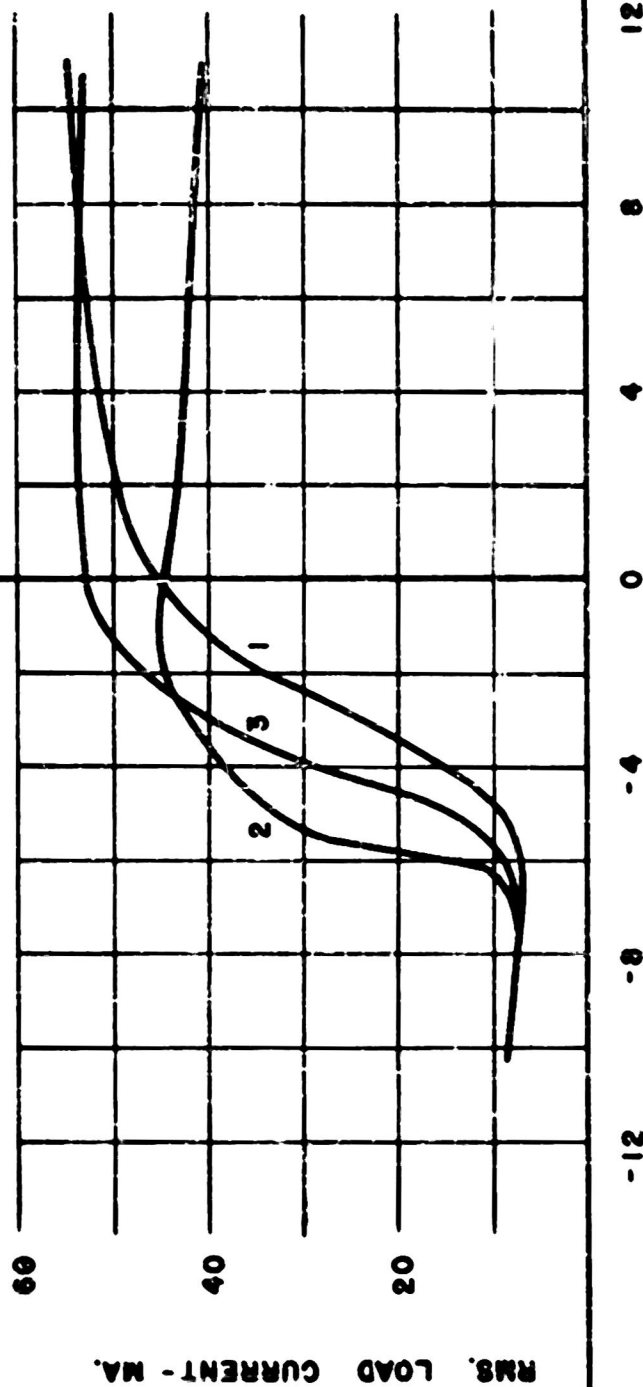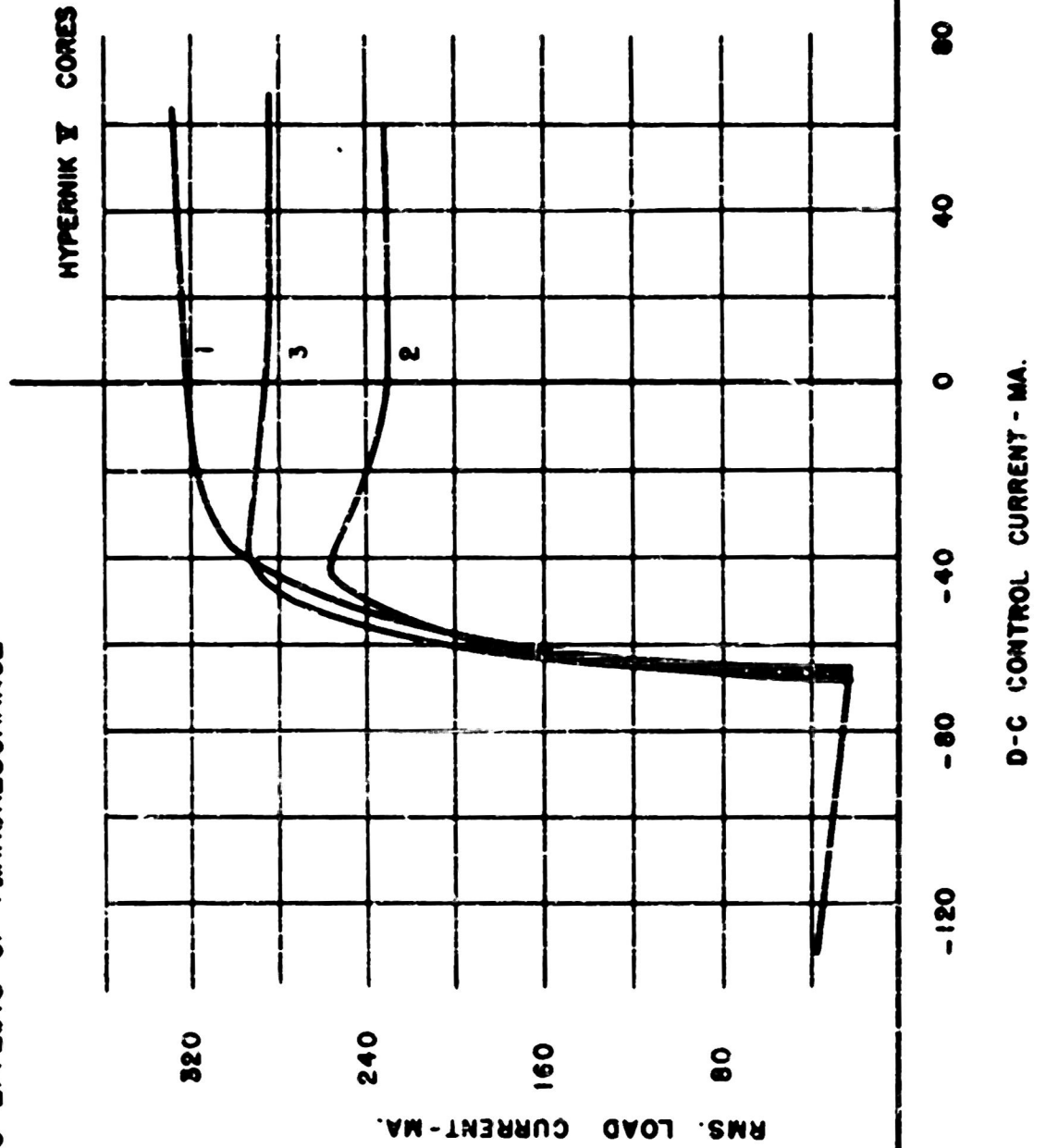ILLUSTRATING EFFECTS OF FERRORESONANCE

HYPERNIK II CORES

$E = 40$ V.
$R_L = 100$ Ohms
60 cps.

1) $C = \infty \mu f$
2) $C = 20$
3) $C = 34$

RMS. LOAD CURRENT - MA.

320

240

160

80

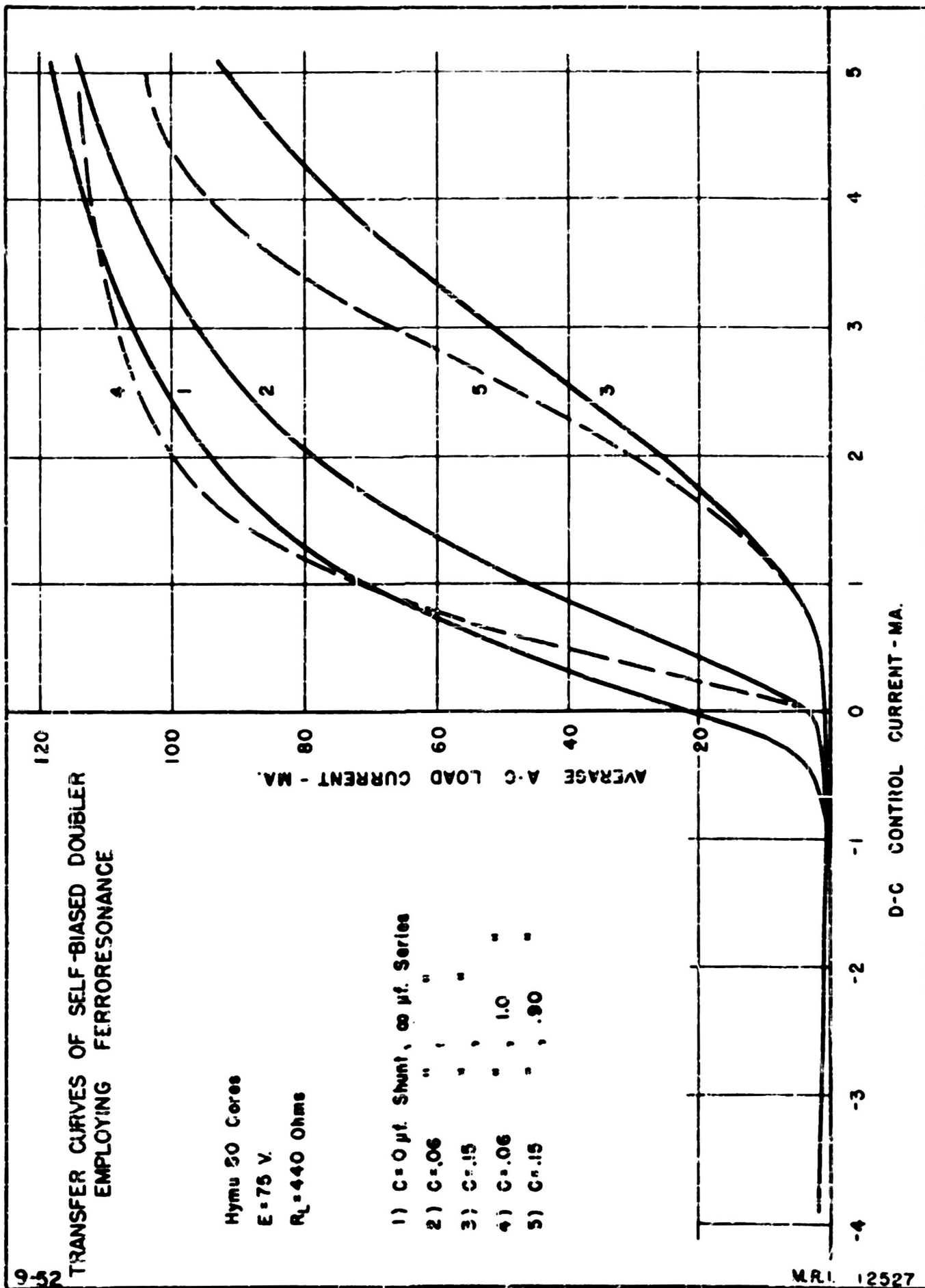D-C CONTROL CURRENT - MA.

-120    -80    -40    0    40    80

G-52

MRI-12526

TRANSFER CURVES OF SELF-BIASED DOUBLER
EMPLOYING FERRORESONANCE

Hymu 80 Cores
E = 75 V.
R_L = 440 Ohms

1) C = 0 μf. Shunt, ∞ μf. Series
2) C = .06   "    "    "    "
3) C = .15   "    "    "    "
4) C = .06   "    "    "  1.0  "
5) C = .15   "    "    "  .90  "

AVERAGE A-C LOAD CURRENT - MA.

D-C CONTROL CURRENT - MA.

9-52

M.R.I. 12527

TRANSFER CURVES OF A DOUBLER EMPLOYING FERRORESONANCE

"Transformer 'C'"  E-I Laminations

E=40 v.

f=400~

R_L=25Ω

(f) = free
(c) = constrained

C=10.8μf. (f)

C=8μf. (c)

C=∞ (f)

C=∞ (c)

AVERAGE LOAD CURRENT – MA.

D.C. CONTROL CURRENT – MA.

9-52

M.R.I.-12528